

Red Supergiant Stars in the Large Magellanic Cloud: I. The Period-Luminosity Relation

Ming Yang and B. W. Jiang

*Department of Astronomy, Beijing Normal University, Beijing 100875, China;
myang@mail.bnu.edu.cn, bjiang@bnu.edu.cn*

ABSTRACT

From previous samples of Red Supergiants (RSGs) by various groups, 191 objects are assembled to compose a large sample of RSG candidates in LMC. For 189 of them, the identity as a RSG is verified by their brightness and color indexes in several near- and mid-infrared bands related to the 2MASS JHKs bands and the *Spitzer*/IRAC and *Spitzer*/MIPS bands. From the visual time-series photometric observations by the ASAS and MACHO projects which cover nearly 8-10 years, the period and amplitude of light variation are analyzed carefully using both the PDM and Period04 methods. According to the properties of light variation, these objects are classified into five categories: (1) 20 objects are saturated in photometry or located in crowded stellar field with poor photometric results, (2) 35 objects with too complex variation to have any certain period, (3) 23 objects with irregular variation, (4) 16 objects with semi-regular variation, and (5) 95 objects with Long Secondary Period (LSP) among which 31 have distinguishable short period, and 51 have a long period shorter than 3000 days that can be determined with reasonable accuracy. For the semi-regular variables and the LSP variables with distinguishable short period, the period-luminosity relation is analyzed in the visual, near-infrared and mid-infrared bands. It is found that the P-L relation is tight in the infrared bands such as the 2MASS JHKs bands and the *Spitzer*/IRAC bands, in particular in the *Spitzer*/IRAC [3.6] and [4.5] bands; meanwhile, the P-L relation is relatively sparse in the V band which may be caused by the inhomogeneous interstellar extinction. The results are compared with others' P-L relationships for RSGs and the P-L sequences of red giants in LMC.

Subject headings: stars: late-type—stars: oscillations—stars: variables: other—supergiants

1. Introduction

Red SuperGiants (RSGs) are evolved, He-burning, extreme Population I stars with moderately high mass ($10\text{-}25 M_{\odot}$) and a degenerate core. They have very large radii ($200\text{-}1500 R_{\odot}$) (Levesque et al. 2005), and spectral types of M or late-K ($T_{\text{eff}} \approx 3000 \sim 4000\text{K}$) (Massey et al. 2008). The very large radii makes them one class of the most luminous stars. Besides, they have

large mass loss rate (MLR) which produces strong stellar wind or even superwind from the outer layer and creates a dusty envelope around the central star. For this reason, RSGs contribute to the interstellar medium, nucleosynthesis and chemical evolution of galaxies (Fusi-Pecci & Renzini 1976; Reimers 1977; Chiosi et al. 1978; Stothers & Chin 1979; Maeder 1981; Chiosi & Maeder 1986; MacGregor & Stencel 1992).

One interesting characteristic of RSGs is that they show optical variability with relatively long period. Some of them are semi-regular variable and referred to as Long Period Variable stars (LPVs). Indeed, LPVs generally include two major types: the Asymptotic Giant Branch stars (AGBs) and the RSGs. Both are luminous with $M_{\text{bol}} \leq -6$ (Wood et al. 1983) and have a variation period ranging from several hundreds to thousand days. The AGB stars often have large amplitude and well-pronounced periodicity while RSGs have small amplitude and not so regular periodicity. A lot of research has been devoted to the study of the long-term variability of RSGs and divided them ambiguously into two groups, the semi-regular and the irregular. The division is ambiguous mostly because of the blurred boundary between the semi-regular and the irregular behavior so that sometimes arbitrary decisions are made for the boundary objects. In the General Catalogue of Variable Stars (GCVS; Kholopov et al. (1985-1988)), SRc and Lc are the two types of RSGs corresponding to the semi-regular and the irregular respectively. Even SRc exhibits two kinds of variation. One is the shorter-period variation characterized by a time scale of several hundreds or less days and identified as the radial pulsation at the fundamental, first and possibly second overtone mode (Stothers 1969; Wood et al. 1983; Lovy et al. 1984; Schaller 1990; Li & Gong 1994; Heger et al. 1997; Guo & Li 2002). The other is the longer-period variation with a period longer than 1000 days, also known as Long Secondary Period (LSP) and found additionally in AGBs and Red Giant stars (RGs) (Stothers 1972; Percy & Bagby 1999; Olivier & Wood 2003; Derekas et al. 2006; Soszyński 2007; Fraser et al. 2008; Wood & Nicholls 2009). The mechanism for this LSP is still unknown. The models like binary, pulsation, convection cell and surface hot spot are proposed but none of them agrees with all the observations and theoretical expectations (Buscher et al. 1990; Wilson et al. 1992; Tuthill et al. 1997; Groenewegen 2004; Wood et al. 2004; Kiss et al. 2006; Messina 2007; Haubois et al. 2009; Nie et al. 2010). Concerning Lc, the irregular variation is considered to be caused by large convection cells which can account for the entire or part of the variation. This scenario is consistent with the profile of the light curve that has an irregular pattern overlying a regular pattern (Schwarzschild 1975; Antia et al. 1984; Kiss et al. 2006).

The difficulty of observing RSGs is the very long time scale of variation. Without multi-cycle coverage of light variation, it is hard even to fully characterize their variation in luminosity, in particular for those with the variation time scale as long as a few thousands of days. Fortunately, with the help of robotic telescopes, long-term photometric monitoring of RSGs is carried out in the past decade which gives us an opportunity to investigate their light variation with a more solid observational base. Kiss et al. (2006) have done a comprehensive study of 48 Galactic RSGs using long-term visual light curves collected by the American Association of Variable Star Observers (AAVSO) with a full span of time of about 60 years. They found semi-regular, irregular variables

and LSPs in their targets. Very recently, using a 10-year photometric monitoring dataset by All Sky Automated Survey (ASAS), Szczygiel et al. (2010) reported their work of discovering 85 semi- or non-periodic RSGs in LMC which are included in our study.

The period-luminosity (P-L) relation of RSGs has aroused much interest. The great intrinsic luminosity of RSGs makes them bright enough to be observed even in distant galaxies. Glass (1979) first discussed the potential of using RSGs as an extragalactic distance indicator. Later, infrared surveys of RSGs in the LMC and SMC by Feast et al. (1980) and Catchpole & Feast (1981) yielded a rough P-L relation. Wood et al. (1983) also made use of infrared JHK photometry and low-dispersion red spectrum to investigate the LPVs in the LMC and SMC. They suggested a criterion to distinguish AGB stars and RSGs by $M_{\text{bol}} = -7.1$, which needs reexamination since some super-AGB stars can be so bright as M_{bol} is up to -8 mag (Poelarends et al. 2008). Nevertheless, they found that RSGs follow a P-L sequence which is approximately one magnitude brighter than AGBs in the K band. Several other groups have studied the P-L relation of RSGs in multiple bands at different distance scales such as in the Milky Way, LMC, SMC and M33 (Feast et al. 1980; Catchpole & Feast 1981; Kinman et al. 1987; Pierce et al. 2000; Kiss et al. 2006). Pierce et al. (2000) re-calibrated the RSG P-L relations in Per OB1, LMC and M33 in various bands and suggested a uniform relation in these heterogeneous environments which can be used to measure the distance to M101. Meanwhile, Kiss et al. (2006), based on the analysis of 48 Galactic RSGs with almost 60-years' data, obtained a P-L relation which is similar to that of AGB stars in LMC. The conclusions from various researchers have some discrepancies, which could be caused by the volume of the sample, the accuracy of the periods or the indicator of the luminosity. In present work, we re-analyze the P-L relation of RSGs in LMC, by carefully selecting a large sample, and by using the most up-to-date photometric data and a few new luminosity indicators.

2. Sample Selection and Data Analysis

First of all, to have a pure and as large as possible sample is the basis to determine a reliable P-L relationship. But this is a difficult task, because RSGs are easily confused with AGB stars since both are red and luminous. Previous works selected the sample of RSGs in LMC by non-uniform criteria. Early in 1980, Feast et al. (1980) identified 24 RSGs from their period and luminosity based on the old Harvard work which included 7 stars from Glass (1979). Wood et al. (1983) produced a new catalog of 26 sources by a detailed analysis of their near-infrared photometry and low-dispersion red spectrum. This catalog became the resource of Pierce et al. (2000) to make their list of 24 RSGs after excluding those which could be AGB stars with a period shorter than 400 days. The sample was largely extended by Massey & Olsen (2003) to be consisted of 158 sources through multi-object spectroscopy of a sample of red stars identified by Massey (2002). They simultaneously made use of high-accuracy ($< 1 \text{ km s}^{-1}$) radial velocities for all the candidates to confirm them as RSGs. Recently, Kastner et al. (2008) selected another sample in a new way, i.e. by choosing the most mid-IR-luminous stars from the 2MASS-*MSX-Spitzer* photometric surveys,

meanwhile Buchanan et al. (2009) had a supplement to this paper that identified additional seven objects as RSGs via their *Spitzer* spectral features and luminosity.

To make a sample as complete as possible, we compiled the samples from Feast et al. (1980), Pierce et al. (2000), Massey & Olsen (2003), and Kastner et al. (2008) altogether as a first step. This preliminary catalog contains in total 232 objects. Actually, these samples overlap, so we adopt the sources by the order of publication to subtract previous sources from following papers. After this, the sample is consisted of 200 stars, specifically 23 from Feast et al. (1980), 11 from Pierce et al. (2000), 140 from Massey & Olsen (2003), and 26 from Kastner et al. (2008).

For the light variation, the time-series photometric data in the visual bands are taken from the databases of the All Sky Automated Survey (ASAS) (Pojmanski 2002) and the MAssive Compact Halo Objects (MACHO) projects (Alcock et al. 1997). Although the Optical Gravitational Lensing Experiment (OGLE) (Szymanski 2005) seems to be a good resource as it also observes LMC for several years, it does not provide useful photometric data due to that all targets are saturated in its I band. The one-epoch near- and mid-infrared photometric data are retrieved from the Two Micron All Sky Survey(2MASS) (Skrutskie et al. 2006) PSC, and the *Spitzer*/SAGE Legacy Program (Meixner et al. 2006) database.

2.1. Color-Magnitude Diagrams and Two-Color Diagrams

Because RSGs are easily confused with bright AGB stars and blue supergiants if judged only from the brightness, we need to examine the sample to make sure that every source in the sample is a true RSG. To identify the RSGs, the basic criterion is the brightness, and modified by the effective temperature. Thus the color-magnitude diagrams (CMDs) and two-color diagrams (TCDs) are the tools. Although they should be red and luminous, RSGs always have heavy dusty envelopes due to large mass loss rate which cause large extinction at shorter wavelengths but much less at longer wavelengths. To avoid the effect of extinction as much as possible, we choose the near- and mid-infrared bands of 2MASS and *Spitzer*/SAGE where the extinction is much smaller than in the optical bands. For the infrared magnitudes, the SAGE Winter '08 IRAC Catalog is selected because it includes the Epoch 1 and Epoch 2 (the SAGE project is composed of two-epoch observations) IRAC images and is already cross-associated with the 2MASS Point Source Catalog (Cutri & 2MASS 2004). This is a highly reliable catalog as a subset of the IRAC Archive catalog through strict selection. In addition, we also use the SAGE Winter '08 MIPS 24 μ m Catalog that is cross-associated with the SAGE Winter '08 IRAC catalog. More details about the SAGE catalogs can be found in Meixner et al. (2006) and the SAGE Data Description Document¹.

The RSG candidates are cross-identified in the SAGE catalog by a 1'' search radius that coincides with the nominal pointing accuracy of *Spitzer* and choosing the closest and brightest

¹<http://irsa.ipac.caltech.edu/data/SPITZER/SAGE/doc/>

counterpart from the objects within the search circle. Actually, because RSGs are of great intrinsic luminosity and located always in sparse stellar field, the $1''$ search radius only results in one counterpart for each source. In addition, even the source has null bands in the 2MASS/JHKs or *Spitzer*/IRAC bands, it is retained other than dropped. Nine targets which have no counterpart in the infrared catalog within the search circle are dropped. As the final SAGE catalogue is yet to be released, the Epoch 1 and Epoch 2 data are still separated, but the differences in the infrared magnitudes between them are less than one percent and negligible. Therefore, we used the Epoch which has more sources and extracted the rest from the other Epoch. For example, the Massey sample has more sources in Epoch 2 in the IRAC bands, while more sources in Epoch 1 in the MIPS bands. As a result, all the sources have photometric measurements for the integral wavelength range covering from the J ($1.2\mu\text{m}$) band to the MIPS $24\mu\text{m}$ band that would give a better identification and comprehensive view of infrared properties of RSGs. Finally, the sample is consisted of 191 sources. Fig. 1 shows the spatial distribution of all the 191 stars superposed on the *Spitzer*/SAGE $8\mu\text{m}$ mosaic image. We note that many stars clump near the 30 Doradus area. Table 1 lists their coordinates and infrared magnitudes, where the ‘—’ symbol denotes the data is missing in the corresponding band, in total, 28 measurements (with 13 at $24\mu\text{m}$) are missing for 21 objects, as well as the resources for photometric data and the reference.

For comparison, we add the 1268 massive stars ($M \geq 8M_{\odot}$) in the LMC from Bonanos et al. (2009). They are collected from literatures and have been identified by the same criteria in the SAGE infrared data as ours.

Fig. 2 is the $J - K_S/K_S$ CMD for all the targets. No interstellar reddening is taken into account, as the extinction in the J and K_S bands is only about 0.2 and 0.06 mag respectively if the suggested $E(B-V)=0.2$ is adopted, comparable to the observational uncertainty. No.53 and No.178 (the ID number in Table 1) without the J and K_S band data are absent in this diagram. In Fig. 2, most RSG candidates locate within a region of $6.5 < K_S < 10$ and $0.5 < J - K_S < 1.6$ which corresponds to the H region of Nikolaev & Weinberg (2000) for the LMC K~M supergiants but has a higher tip. This means that our sample extends to more luminous sources.

For identification, we set the boundaries of luminosity and color index. According to the mass-luminosity relation for massive stars ($9 - 30M_{\odot}$), $L/L_{\odot} = (M/M_{\odot})^{\gamma}$ with γ very close to 4.0 (Stothers & Leung 1971), the luminosity range of RSGs is $10^4 - 25^4 L_{\odot}$ with the mass range $10 - 25M_{\odot}$, which can be converted to the absolute bolometric magnitude $M_{\text{bol}} = 4.74 - 2.5 \log(L/L_{\odot})$ to range from -9.58 to -5.26. Furthermore, M_{bol} is converted to the K band magnitude from $m_{\text{bol}} = m_K + 3$ (Josselin et al. 2000). A distance modulus of 18.41 mag (Macri et al. 2006) is used to convert the observed K_S to the absolute magnitude. Because the difference of magnitude between the K and K_S bands is very small and can be ignored, we finally get the K_S band magnitude should be between 5.83 mag and 10.15 mag, shown as the dashed horizontal lines in Fig 2. For the color index $J - K_S$, the lower limit is 0.5, the same as the lower observational boundary of Josselin et al. (2000) and the upper limit is 1.6, the same as the boundary of carbon-rich stars defined by Hughes & Wood (1990). These limits also are consistent with the color indexes of most

candidates. Additionally marked by dotted line in Fig. 2 is the criterion of $M_{\text{bol}} = -7.1$ which was proposed to distinguish the AGBs and RSGs by Wood et al. (1983). It can be seen that this criterion would leave a third of our targets out and difficult to reconcile with others. Besides clustering in Fig. 2, the RSGs exhibit an upward tendency toward the red end in $J - K_S$, which indicates a higher mass loss rate at higher K_S luminosity. This tendency becomes clearer at longer wavelengths in subsequent analysis. The broadening of the sequence may be caused by different MLR. In this CMD, there are a few candidates lying outside the boundaries. In the far upright of this figure are No.2 and No.167, they exceed a little bit the upper limit of $J - K_S = 1.6$. No.58 is too faint to satisfy the lower limit of K_S band luminosity.

From Fig. 2, the identification of the RSG candidates is almost finished. Meanwhile, RSGs are in the evolved phase and have large MLR. Several authors observed that RSGs have circumstellar dust features from $8\mu\text{m}$ to $12\mu\text{m}$ (Hagen 1978; Skinner & Whitmore 1988; Josselin et al. 2000), mainly the $9.7\mu\text{m}$ silicate feature and the $12.1\mu\text{m}$ feature. Therefore, in order to further confirm the identification of RSGs, the color index involving a MIR band should be helpful.

In Fig. 3, the targets are plotted in the $K_S - [8.0]/[8.0]$ CMD. Nos. 53, 58 and 178 lack the K_S and/or [8.0] band data, they are not present in this diagram. Because no ready-made criterion can be used on these bands, we set our own limits for RSGs to include 98% clumped targets, which means: $5.3 \leq [8.0] \leq 9.7$ and $0.1 \leq K_S - [8.0] \leq 2.0$. Here are again a couple of outliers, No.2 and No.167 are still in the far right and a new outlier obviously redder than the others in the right side is No.132.

Aside from the [8.0] band, the MIPS [24] band also reflects the emission of the dust, but the cooler dust (Blum et al. 2006; Bonanos et al. 2009). Fig. 4 shows the $[8.0] - [24]/[24]$ CMD. No.53 lacks the [8.0] band data, No.58 lacks the [8.0] and [24] band data, Nos.8, 73, 75, 93, 117, 147, 161, 167, 169, 182, 184 and 189 lack the [24] band data, they are absent in this diagram. The targets are divided clearly into two groups. The targets from Kastner et al. (2008), Pierce et al. (2000) and Feast et al. (1980) have redder [8.0]-[24] and thus are RSGs with colder dust, while the targets from Massey & Olsen (2003) have bluer [8.0]-[24] and are RSGs with warmer dust. The two groups share similar luminosity in [24] at the high end. But the redder group do not extend to the faint end, which is true in [8.0] as well, while not true in K_S since the stellar radiation is the main contributor in near-infrared. The consistency at the short wavelengths indicate that the stars of the two groups are more or less of the same luminosity, while the difference at the long wavelengths is caused only by the amount and temperature of dust. So both groups should be RSGs, but with different dust. As done in previous diagram, we also give the empirical limits for RSGs as $3.2 \leq [24] \leq 9.5$ and $0.1 \leq [8.0] - [24] \leq 3.0$. Then, there are four outliers. No.2 and No.13 are a little bit brighter than other targets. No.56 is bluer and No.178 is redder than the major group. But since the [24] band mainly reflects the characteristic of circumstellar dust other than the central star, the variation of color index should be the influence of dust temperature which does not directly relate to the central star.

Bonanos et al. (2009) showed that RSGs locate in a distinct region in a couple of TCDs. As an example, Fig. 5 is the [3.6]-[4.5]/[4.5]-[8.0] TCD. RSGs locate in a region with [3.6]-[4.5] bluer than other luminous red stars, which is due to the depression at [4.5] by the CO bands around $4.6\mu\text{m}$ (Verhoelst et al. 2009). Nos.51, 53, 58, 70, 82, 98, 129, and 181 are not present in this diagram due to lack of the measurement in related bands. There are apparently three outliers, No.2, No.167 and No.178.

Combining the information from the CMDs and TCDs, we exclude No.2 and No.167 for their inconsistent colors and luminosities. A few marginal cases are retained, i.e. No.56 and No.178, because they stay together with the majority of RSGs in some of the diagrams.

From the CMDs and TCDs, it can be seen that there are about two dozens massive sources from Bonanos et al. (2009) which locate in the same regions in these diagrams as RSGs but are not included in the sample. These sources are not included in previous studies like spectroscopy or detailed analysis, but they may be RSGs judged from their luminosity and colors. Further observations are needed. This shortage indicates that the present sample of RSGs is not complete, but seems to include most RSGs.

2.2. Period Determination and Analysis

To collect as long as possible light curves which would make more accurate period determination, we browsed the online databases of the ASAS and MACHO projects to search for all useful data. Most of our photometry data comes from ASAS because RSGs, except several heavy-envelop-surrounding targets with excess visual extinction, easily get saturated in the MACHO observation due to their great intrinsic luminosity (Massey et al. 2005). The V magnitude is expected to be brighter than about 14 mag for RSGs in LMC, estimated from the minimum mass of RSGs and the distance modulus of LMC, while the saturation limit is on average about 13 mag in the Kron-Cousins V band and about 14 mag in the R band (Kem Cook, private communication) for the MACHO project. Sometimes, an abnormal light curve is still retrieved from the MACHO database for a target even it is saturated. As the saturation magnitude depends on the seeing, the MACHO photometry code SoDOPHOT (basically DoPhot) can measure more photo-electrons for a stellar image at worse seeing than average condition. But for this to work, the template image should not be saturated. The abnormal light curve is indeed caused by the saturated template image. Thus, all abnormal light curves are dropped. The photometric precision of MACHO is about 0.02 magnitude, as an internal error, in both bands of its own two-color system in field-overlap regions for the brightness between 13 ~ 18 mag in the V band (Alcock et al. 1999). ASAS has an average precision of about 0.05 mag, but in some cases (due to problems with flat-fielding and lack of color information) the errors could be 0.1 magnitude or larger (Pojmanski 2002). Although the ASAS photometric precision is slightly lower than the MACHO project, it better fits the high luminosity of RSGs and the numerous observations can compensate partly for the precision. In addition, by deleting the low-quality data, the ASAS data have reasonably good precision and time coverage to

derive typical optical variation properties of RSGs.

The way to handle the photometric data depends on the datasets. For ASAS, the standard Johnson V band data are used since the released continuous I band data cover only about 500 days. Because the search radius is fixed as $30''$ to retrieve the photometric data from the project website, it does need to check the DSS image for the input coordinates how many stars fall into the search circle. For the coordinates of each target, the counterpart is accepted only when its distance to the target is less than $10''$ and its average V band magnitude brighter than 14 mag (for a good S/N to be achieved by ASAS) (Grzegorz Pojmanski, private communication). The criteria exclude 16 targets with large coordinate deviations and 14 targets with more than two sources in the $10''$ circle. Moreover, the processed online ASAS data are graded into four levels marked by A to D that indicate the photometric quality for each aperture, and we only make use of the A data with the best quality. We also removed the points which lay more than 3σ away from a resistant estimate of the dispersion of the light curve distribution, where σ is the standard deviation (Hoaglin et al. 1983). This selection removes most of the outlying points. Except some poor photometric measurements, there are 161 targets with ASAS data useful. Among them, according to the previous identifications based on the CMDs and TCDs, No.2 has large coordinate deviation and No.167 has good photometry. After excluding No.167, 160 targets have ASAS data available. Then the least-square (Savitzky-Golay) polynomial smoothing filter is applied to the light curve, which would reduce noise greatly in the time-series data but retain dynamic range of variations in the data (Press et al. 1992). The process of handling the ASAS photometric data is shown in the left column of Fig. 6 for one target.

For MACHO, the non-standard two-color photometric system magnitudes are transformed to the standard Kron-Cousins V and R system by modifying the formulae of Alcock et al. (1999) as $V = V_{M,t} + a_0 + 1.089(a_1 + 0.022X_t) + c_0 + 2.5 \log(ET)$ and $R = R_{M,t} + b_0 + 1.089(b_1 + 0.004X_t) + c_0 + 2.5 \log(ET)$ in which the arithmetic average of V-R=1.089 of RSGs is adopted from Levesque et al. (2006). The search radius is $3''$ thanks to the high-accuracy positioning system and the large aperture of the MACHO telescope. The MACHO project finally provides the photometric data for 18 targets. Among them, 9 targets do not have ASAS data due to the coordinate deviation and the others have useful ASAS photometry data. The outliers in the CMDs and TCDs in previous section do not have any MACHO data available. Because of the low temperature and thick envelope, RSGs are usually quite red and brighter in the R band than in the V band. They are easily saturated in the R band and left with only the K-C V band data useful. In the process to convert the template magnitude to the standard system, the correction for the air mass, if following the average parameters of the system, would bring about large uncertainty in the case of large air mass, which can be understood as the atmosphere changes greatly from night to night. The data points with airmass larger than 2.0 are thus deleted, which does not affect the accuracy of the period significantly as the measurements for every source are numerous. Besides, the measurement with photometric error bigger than 0.2 mag is also removed. At last, combining the ASAS and MACHO data, 169 targets have the photometry data available and useful. The resource for each

target is labeled by 'M' for MACHO and 'A' for ASAS in Table 1.

RSGs are found to be variable for long time. But their variation is not very regular, which makes the period determination a tough task. On the other hand, an accurate determination of the period is the key to the period-luminosity relation. In order to be certain about the period, a couple of methods are used to obtain the most consistent period.

First, a simple and effective way, the Phase Dispersion Minimization (PDM) method (Stellingwerf 1978), is used to find the light variation period. In brief, the PDM method folds the data at a range of trying periods, divides the folded data into a series of bins and computes the variance of the amplitude within each bin. The bin variances are combined and compared to the overall variance of the data set. For a true period, the ratio of the bin to the total variances, defined as theta (Θ), should be the minimum and for a false period the ratio is approximately unity. This method is very useful in particular for data sets with gaps and non-sinusoidal variations. Since the light variation of RSGs is mostly non-sinusoidal, PDM is an appropriate technique. There is an empirical tip when using this method, i.e., one should estimate the rough period range via eyes, because the harmonics of the periods would also produce very small theta, even smaller than the theta value at the true period. A sample of the PDM processing is shown in the right column in Fig. 6.

Although PDM is an outstanding method to detect the light variation period, there are still some obstacles. A major problem is that our data has a time span of about 3000 days which is sufficient to determine the moderately long periods, but not long enough for the periods over 1500 days because the time coverage is less than two periods. Actually, Long Secondary Periods (LSPs) which are found in the AGBs and RGs variables are also present in RSGs. The LSPs are often thousands of days long, sometimes exceeding the time span of the data set and leading to an unreliable period determination by PDM. In such case, the Period04 (Lenz 2004) method based on the Fourier transform works better. So, in addition to the PDM method, Period04 is also used to analyze the variability of the targets. One purpose of using Period04 is to extract the long LSP in some cases, the other is to confirm the period derived from PDM. For the later purpose, Period04 implements iterative sinusoid fitting to fit and subtract a sinusoid match with the frequency at the highest peak in power spectrum in each iteration. After first iteration, the residual data are used to calculate the power spectrum in the following iterations. The iteration is stopped until the highest peak in the residual spectrum is less than four times of the noise level. A sample of Period04 processing is shown in Fig. 7. Only when the periods derived from PDM and Period04 agree with each other, is the period regarded as true. Fig. 8 shows a comparison of the periods derived from PDM and Period04, and the inset is the histogram of the difference between these two periods for 47 RSGs. It can be seen that the difference is mostly less than 10 days. From the consistency between PDM and Period04, the period is regarded to be real.

3. Period-Luminosity Relation

According to the analysis of the time-series photometric data, the targets are divided into five categories. The first category includes 20 RSGs. They are either too bright and saturated in photometry or in a crowded stellar field or having a close companion impossible to resolve. These stars have poor photometry data and are not considered for any further analysis. The second category includes 35 RSGs which have complex lightcurve not suitable for deriving the P-L relation. The third category includes 23 RSGs. They are irregular variables, for which there is no possibility to find an appropriate period to characterize its light variation. They are neither considered for further study of the P-L relation in the following part of this paper. But they are the characters in our next paper on the period change of RSGs. The remaining 111 RSGs are semi-regular or LSP RSGs which are involved in the following determination of the P-L relation and classified into the fourth and fifth categories. The fourth category includes 16 RSGs, being semi-regular variables with period statistical significance less than or equal to 0.05. Among them, 4 targets are in Feast et al. (1980), 1 in Pierce et al. (2000), 4 in Kastner et al. (2008) and 7 in Massey & Olsen (2003). One thing to keep in mind is that there is no clear borderline between semi-regular and irregular variables. What we do is to calculate the statistical significance of the period corresponding to the minimum theta and classify the object as a semi-regular variable when the significance is smaller than 0.05 (Schwarzenberg-Czerny 1997). The fifth category includes 95 RSGs which have LSP, 31 of them have distinguishable short period. For the 16 semi-regular variable RSGs and those 31 LSP RSGs but with distinguishable short period, the period can be determined with relatively high accuracy, and suitable for discussing the P-L relation. Their periods are derived and the results are shown in Table 2. For an intuitive view, we give the irregular, semi-regular and LSP RSGs each a sample light curve in Fig. 9.

We also calculate the linear relation of amplitude with period for the RSGs present in Table 2. The result is $\Delta V = (1.74 \pm 0.54) \times P - (4.25 \pm 1.13)$, with rms=0.74, where ΔV is the full amplitude in the V band and P is the period. This is consistent with the general tendency of variables that the longer the period the greater the amplitude. The distribution of the full amplitude with the period is shown in Fig. 10. The average period $\bar{P} = 618$ day and the average amplitude in the V band $\Delta \bar{V} = 0.698$ mag.

Beside the period, the other key parameter in the P-L relation is the luminosity. Usually the luminosity is derived from the brightness in one specific band by converting through the bolometric correction. The band often used is the visual V band or the near-infrared K band. Such method has to suffer the bolometric correction factor that is relatively uncertain for RSGs. The V band further suffers the interstellar extinction from both the Galaxy and the LMC, and even the circumstellar dust, which may be serious and more importantly is inhomogeneous. The choice of the indicator of the luminosity has to be cautious.

As a trying, the period is plotted against the brightness in various bands, the visual band V , the near-infrared band K_s and the *Spitzer*/IRAC bands. The V band completely reflects the radiation

of the stellar photosphere, but it can be seriously affected by extinction ($A_V=0.6$ mag at $E(B-V)=0.2$ for the Galactic extinction at the direction to LMC), in particular the targets should experience inhomogeneous extinction because they locate in different environments in LMC, which can be seen in Fig. 1. Even if we correct the foreground Galactic interstellar extinction, it is impossible to correct the extinction of LMC since we are neither clear about the extinction structure of LMC nor the depth of the targets. So no interstellar extinction is corrected in any band, this for sure underestimates the luminosity, much in visual bands, a little in near-infrared bands, and little in *Spitzer*/IRAC bands. Meanwhile, the brightness in the *Spitzer*/IRAC long-wavelength band [8.0] must be at least partly from the emission of the surrounded dust so that it is not a right indicator of the stellar luminosity, but it has the advantage of best avoiding the effect of interstellar extinction. In spite of such various shortcomings, the linear analysis of the P-L relation is performed to every band involved in the way $M_\lambda = a \log P + b$. The slope a and intercept b with their dispersions are listed in Table 3, and the fitted lines are shown in Fig. 11 and Fig. 12.

The period-luminosity relationship does exist in the semi-regular RSG variables and the LSP with distinguishable short period in all bands, but the amount of dispersion depends on the band. In the V band the dispersion is the biggest. In the J band, and the MIPS [24] and [8.0] bands, the dispersion is relatively big, but the P-L relations are reasonably good. In the H, K, [3.6] and [5.8] bands, the dispersion is very small, and the P-L relation is very tight. The best relationship occurs in the [4.5] band. However, with very small difference, the later two groups, i.e. H, K, [3.6], [4.5] and [5.8], all have a highly reliable P-L relation. This can be understood. In these bands, their brightness should come mainly from the stellar photosphere if the targets are cold and have no thick dust envelope. Besides, the extinction is very small in these bands. According to the newest estimation of extinction in the IRAC bands, the extinction in the [3.6] and [4.5] bands is only 63% and 57% of the K band extinction (Gao et al. 2009), which means only about 0.04 mag at $E(B-V)=0.2$ for the Galactic foreground extinction, significantly smaller than the photometric error. Moreover, the variation amplitude in the infrared should be very small from the decreasing tendency of the amplitude with the wavelength, so that the one-epoch magnitude can represent the average brightness very approximately. Therefore, with the large-scale data available from *Spitzer*, the short IRAC bands are recommended as the luminosity indicator.

In the K_S band, previous investigators already obtained the P-L relation for RSGs. In Fig. 13, our result is compared with the P-L relation for RSGs in LMC by Feast et al. (1980) and in the Per OB1 association, LMC and M33 by Pierce et al. (2000). It can be seen that our result doesn't agree perfectly with either of them, but close to that of Pierce et al. (2000), and very different from that of Feast et al. (1980). Our result is also compared with the P-L relation for RSGs in our Galaxy by Kiss et al. (2006). Our result brings about systematically fainter luminosity than Kiss et al. (2006), indeed, the Kiss et al. (2006) relation produces higher luminosity at a given period than that of Feast et al. (1980) and Pierce et al. (2000) as well. However, our P-L relation is almost perfectly matched with the extension of the AGB a_2 sequence of Soszynski et al. (2007), where the objects are the so-called OGLE Small Amplitude Red Giants (OSARGs), corresponding to the sequence B

of Wood et al. (1999) and identified as the first overtone radial pulsating red giants. But whether these RSGs are pulsating in the first overtone mode needs further proof because no other sequences such as the fundamental and second overtone modes are accompanied.

As the LSP is also a periodic phenomenon, the LSP RSGs are checked whether the P-L relation exists. The periods of LSP RSGs are calculated from the power density spectrum using the Period04 code (Lenz 2004). The periods and amplitudes in the V-band of these RSGs are shown in Table 4, where only 51 targets with the period shorter than 3000 days are listed, while the other 44 RSGs have very possibly a longer period exceeding the length of the data set that makes the period determination uncertain. It can be told that they have periods of a few thousand days, much longer than that of the semi-regular RSGs, expected from their identity as Long Secondary Period variables. Besides, the amplitude of variation is only a few tenths magnitude, much smaller than that of the semi-regular RSGs. Both the period and amplitude indicate that the LSP RSGs are a different type of variables from the semi-regular RSGs. Their origin of variation should be different too. Indeed, the origin of LSP in semi-regular variable Miras is very controversial. Many models, including radial and non-radial pulsation, binary, stellar spot models, are suggested but none of them receives general acceptance (Wood & Nicholls 2009; Nie et al. 2010). For the LSP in RSGs, it has not even attracted much attention except for Kiss et al. (2006). The data covering much longer time are the key to study the behavior of the LSP of RSGs. With the continuation of the ASAS project, a more reliable determination of the period and analysis of the mechanism are promising.

For an overview of the P-L relation of the semi-regular and the LSP RSGs, Fig. 14 shows their period and brightness in the K_s band in comparison with the P-L relations of red giants by Soszynski et al. (2007). It again exhibits an almost perfect match with the extension of the Soszynski a_2 sequence, and the LSP lies between the C and D sequences. Different from the red giants, the RSGs do not form well-defined sequences. The technical reason may be the smallness of the sample and the relatively short duration of the time series. But the irregularity of the variation of RSGs brings about the difficulty in determining period and the dispersion of the relation as well.

4. Summary

The P-L relation of RSGs has been known to exist that gives an opportunity to extend the distance calibration from these luminous and reasonably numerous targets. With the latest optical and infrared survey data, we obtained a series of period-luminosity relations in several infrared bands, new or different from previous studies.

The preliminary sample of RSGs is ever the largest by combining a few systematic samples. To obtain a reliable match, the infrared data of our sample are selected by strict criterion with a one-arcsec search radius with the *Spitzer*/IRAC and MIPS databases. Although this criterion drops some targets with a little big position error, the loss in the size of the sample is acceptable from the original large sample. The final sample consists of 191 sources. To further purify the

sample to be consisted of only RSGs, two more targets are dropped because they have slightly different colors and luminosity from the bulky members according to their locations in a few CMDs and TCDs.

The time-series photometric data are mainly taken from the ASAS project, supplemented by the MACHO project. Usually more than 300 measurements are available for one target and the time span is longer than a few thousand days. The period analysis is performed carefully by the PDM method and further checked by the Period04 code for consistency. Based on the derived period and amplitude as well as the shape of light curve, the RSGs are classified into five categories: 20 RSGs saturated in photometry or located in crowded stellar field, 35 RSGs with complex light curve, 23 RSGs with irregular variation, 16 RSGs with semi-regular variation, 95 RSGs with LSPs among which 31 have distinguishable short period, and 51 have a long period shorter than 3000 days that can be determined with reasonable accuracy while the remaining 44 objects have a long period exceeding the length of the data set.

The P-L relation is found to exist both in the semi-regular variable and LSP RSGs with distinguishable short period. This relationship is analyzed in various bands, from visual V , through near-infrared JHK_S , to the mid-infrared *Spitzer*/IRAC/MIPS bands. Except the V band, the P-L relation is tight in all the other bands, and it has the least dispersion in the IRAC [3.6] and [4.5] bands that are recommended for use.

For the derived P-L relation, some attentions must be paid. First, the sample has 191 RSGs, but only 47 obey the P-L relation, i.e. 24%. It means that many RSGs do not obey the P-L relation. Before making use of the P-L relation, for example as a distance calibrator for distant galaxies, one must make sure that the tracer RSG has an accurately determined period. Moreover, the P-L relation is tighter at longer wavelengths, 3.6 and 4.5 micron in our cases, which is not affected significantly by not only interstellar extinction but also the surrounded dust of RSG itself. For this purpose, the photometry in such bands are needed.

Our work is roughly consistent with Pierce et al. (2000) in the K-band P-L relation but with better precision at longer wavelengths. Pierce et al. (2000) gave a simultaneous fitting for RSGs in the Per OB1 association of the Galaxy, LMC and M33 which may participate more uncertainty in this relation. The difference with Kiss et al. (2006) could be due to the difference in the metallicity between Galaxy and LMC or the methods in period determination.

5. Acknowledgements

We thank Prof. P. Wood for very helpful discussion, and the anonymous referee for useful suggestions. This work is supported by China's NSFC through the projects 10778601 and 10973004, China 973 Program 2007CB815406, and the Fundamental Research Funds for the Central Universities.

REFERENCES

- Alcock, C., et al. 1997, *ApJ*, 486, 697
- Alcock, C., et al. 1999, *PASP*, 111, 1539
- Antia, H. M., Chitre, S. M., & Narasimha, D. 1984, *ApJ*, 282, 574
- Blum, R. D., et al. 2006, *AJ*, 132, 2034
- Bonanos, A. Z., et al. 2009, *AJ*, 138, 1003
- Buchanan, C. L., Kastner, J. H., Hrivnak, B. J., & Sahai, R. 2009, *AJ*, 138, 1597
- Buscher, D. F., Baldwin, J. E., Warner, P. J., & Haniff, C. A. 1990, *MNRAS*, 245, 7P
- Catchpole, R. M., & Feast, M. W. 1981, *MNRAS*, 197, 385
- Chiosi, C., Nasi, E., & Sreenivasan, S. R. 1978, *A&A*, 63, 103
- Chiosi, C., & Maeder, A. 1986, *ARA&A*, 24, 329
- Cutri, R. M., & 2MASS 2004, *Bulletin of the American Astronomical Society*, 36, 1487
- Derekas, A., Kiss, L. L., Bedding, T. R., Kjeldsen, H., Lah, P., & Szabó, G. M. 2006, *ApJ*, 650, L55
- Feast, M. W., Catchpole, R. M., Carter, B. S., & Roberts, G. 1980, *MNRAS*, 193, 377
- Fraser, O. J., Hawley, S. L., & Cook, K. H. 2008, *AJ*, 136, 1242
- Fusi-Peccì, F., & Renzini, A. 1976, *A&A*, 46, 447
- Gao, J., Jiang, B. W., & Li, A. 2009, *ApJ*, 707, 89
- Glass, I. S. 1979, *MNRAS*, 186, 317
- Groenewegen, M. A. T. 2004, *A&A*, 425, 595
- Guo, J. H., & Li, Y. 2002, *ApJ*, 565, 559
- Hagen, W. 1978, *ApJS*, 38, 1
- Haubois, X., et al. 2009, *A&A*, 508, 923
- Heger, A., Jeannin, L., Langer, N., & Baraffe, I. 1997, *A&A*, 327, 224
- Hoaglin, D. C., Mosteller, F., & Tukey, J. W. 1983, *Wiley Series in Probability and Mathematical Statistics*, New York: Wiley, 1983, edited by Hoaglin, David C.; Mosteller, Frederick; Tukey, John W.,

- Hughes, S. M. G., & Wood, P. R. 1990, *AJ*, 99, 784
- Josselin, E., Blommaert, J. A. D. L., Groenewegen, M. A. T., Omont, A., & Li, F. L. 2000, *A&A*, 357, 225
- Kastner, J. H., Thorndike, S. L., Romanczyk, P. A., Buchanan, C. L., Hrivnak, B. J., Sahai, R., & Egan, M. 2008, *AJ*, 136, 1221
- Kiss, L. L., Szabó, G. M., & Bedding, T. R. 2006, *MNRAS*, 372, 1721
- Kholopov, P.N., et al., 1985-1988, *General Catalogue of Variable Stars*, 4th edition, Nauka, Moscow
- Kinman, T. D., Mould, J. R., & Wood, P. R. 1987, *AJ*, 93, 833
- Lenz, P. 2004, *Communications in Asteroseismology*, 144, 41
- Levesque, E. M., Massey, P., Olsen, K. A. G., Plez, B., Josselin, E., Maeder, A., & Meynet, G. 2005, *ApJ*, 628, 973
- Levesque, E. M., Massey, P., Olsen, K. A. G., Plez, B., Meynet, G., & Maeder, A. 2006, *ApJ*, 645, 1102
- Li, Y., & Gong, Z. G. 1994, *A&A*, 289, 449
- Lovy, D., Maeder, A., Noels, A., & Gabriel, M. 1984, *A&A*, 133, 307
- Macri, L. M., Stanek, K. Z., Bersier, D., Greenhill, L. J., & Reid, M. J. 2006, *ApJ*, 652, 1133
- MacGregor, K. B., & Stencel, R. E. 1992, *ApJ*, 397, 644
- Maeder, A. 1981, *A&A*, 99, 97
- Massey, P. 2002, *ApJS*, 141, 81
- Massey, P., & Olsen, K. A. G. 2003, *AJ*, 126, 2867
- Massey, P., Plez, B., Levesque, E. M., Olsen, K. A. G., Clayton, G. C., & Josselin, E. 2005, *ApJ*, 634, 1286
- Massey, P., Levesque, E. M., Plez, B., & Olsen, K. A. G. 2008, *IAU Symposium*, 250, 97
- Meixner, M., et al. 2006, *AJ*, 132, 2268
- Messina, S. 2007, *New A*, 12, 556
- Nie, J. D., Zhang, X. B., & Jiang, B. W. 2010, *AJ*, 139, 1909
- Nikolaev, S., & Weinberg, M. D. 2000, *ApJ*, 542, 804
- Olivier, E. A., & Wood, P. R. 2003, *ApJ*, 584, 1035

- Percy, J. R., & Bagby, D. H. 1999, *PASP*, 111, 203
- Pierce, M. J., Jurcevic, J. S., & Crabtree, D. 2000, *MNRAS*, 313, 271
- Poelarends, A. J. T., Herwig, F., Langer, N., & Heger, A. 2008, *ApJ*, 675, 614
- Pojmanski, G. 2002, *Acta Astron.*, 52, 397
- Press, W. H., et al., *Numerical Recipes*, 2nd ed. (Cambridge University Press, Cambridge, England), 1992, Sec. 14.8, p. 650
- Reimers, D. 1977, *A&A*, 57, 395
- Schaller, G. 1990, *Confrontation Between Stellar Pulsation and Evolution*, 11, 300
- Schwarzenberg-Czerny, A. 1997, *ApJ*, 489, 941
- Schwarzschild, M. 1975, *ApJ*, 195, 137
- Skinner, C. J., & Whitmore, B. 1988, *MNRAS*, 235, 603
- Skrutskie, M. F., et al. 2006, *AJ*, 131, 1163
- Soszynski, I., et al. 2007, *Acta Astron.*, 57, 201
- Soszyński, I. 2007, *ApJ*, 660, 1486
- Stellingwerf, R. F. 1978, *ApJ*, 224, 953
- Stothers, R. 1969, *ApJ*, 156, 541
- Stothers, R., & Leung, K. C. 1971, *A&A*, 10, 290
- Stothers, R. 1972, *A&A*, 18, 325
- Stothers, R., & Chin, C.-W. 1979, *ApJ*, 233, 267
- Szymanski, M. K. 2005, *Acta Astron.*, 55, 43
- Szczygiel, D. M., Stanek, K. Z., Bonanos, A. Z., Pojmański, G., Pilecki, B., & Prieto, J. L. 2010, *AJ*, 140, 14
- Tuthill, P. G., Haniff, C. A., & Baldwin, J. E. 1997, *MNRAS*, 285, 529
- Verhoelst, T., van der Zypen, N., Hony, S., Decin, L., Cami, J., & Eriksson, K. 2009, *A&A*, 498, 127
- Wilson, R. W., Baldwin, J. E., Buscher, D. F., & Warner, P. J. 1992, *MNRAS*, 257, 369
- Wood, P. R., Bessell, M. S., & Fox, M. W. 1983, *ApJ*, 272, 99

Wood, P. R., et al. 1999, *Asymptotic Giant Branch Stars*, 191, 151

Wood, P. R., Olivier, E. A., & Kawaler, S. D. 2004, *ApJ*, 604, 800

Wood, P. R., & Nicholls, C. P. 2009, *ApJ*, 707, 573

Table 1. Infrared brightness of the 191 RSG candidates

No.	RA (°)	Decl (°)	J	H	K _S	[3.6]	[4.5]	[5.8]	[8.0]	[24]	Data ^a	Reference ^b
1	72.343634	-69.409571	9.052	8.171	7.763	7.376	7.297	7.036	6.480	3.980	A	K
2	72.422868	-68.630874	9.130	8.047	7.486	6.919	6.522	6.096	5.032	2.796	—	K
3	72.744524	-69.234115	9.433	8.603	8.355	8.008	8.247	8.000	7.886	6.638	A	M
4	72.879183	-69.247765	9.426	8.549	8.239	7.951	8.165	7.919	7.804	6.415	A	M
5	72.947048	-69.323501	9.863	9.033	8.740	8.539	8.711	8.526	8.325	7.047	A	M
6	73.311619	-69.204979	9.143	8.134	7.751	7.514	7.563	7.299	7.053	4.975	A	M
7	73.326893	-69.284163	9.517	8.670	8.356	8.098	8.274	8.020	7.650	7.092	A	M
8	73.378763	-69.297135	9.321	8.457	8.056	7.491	7.458	7.117	6.519	—	A	K
9	73.653572	-69.339499	8.332	7.832	7.614	7.329	7.454	7.283	7.080	6.038	A	M
10	73.660602	-69.188074	8.543	7.662	7.203	6.869	6.659	6.340	5.696	3.942	A	M
11	73.664248	-69.076768	9.808	9.026	8.662	8.288	8.218	7.935	7.569	5.338	A	P
12	73.707049	-69.500735	9.484	8.728	8.429	8.122	8.177	7.939	7.720	6.847	A	M
13	73.762753	-69.486868	8.658	7.685	7.200	6.714	6.454	6.125	5.499	2.830	A	K
14	73.816926	-69.320038	8.558	7.751	7.374	7.123	7.181	6.885	6.352	4.982	A	M
15	73.840164	-69.787996	8.925	7.950	7.618	7.500	7.254	6.919	6.351	3.744	A	K
16	73.875008	-69.486257	8.696	7.965	7.658	7.337	7.426	7.119	6.781	4.974	A	M
17	73.883554	-66.843868	8.680	7.921	7.661	7.329	7.325	7.073	6.757	4.772	A	P
18	73.895278	-69.448796	8.233	7.448	7.113	6.857	6.946	6.581	6.063	3.961	A	K
19	73.924266	-69.440054	8.800	8.026	7.695	7.449	7.485	7.218	6.831	4.537	A	P
20	73.951116	-69.401813	9.127	8.280	7.968	7.710	7.925	7.618	7.210	5.180	A	M
21	74.098594	-69.703102	9.512	8.701	8.454	8.232	8.448	8.266	8.136	6.941	A	M
22	74.117827	-69.676949	9.504	8.657	8.427	8.148	8.330	8.184	8.050	6.702	A	M
23	74.381387	-70.149824	9.157	8.291	7.973	7.474	7.356	7.074	6.645	4.313	A	P
24	74.430466	-70.147335	8.436	7.648	7.324	6.742	6.736	6.442	5.965	3.433	A	F
25	74.435802	-69.509524	9.694	8.849	8.562	8.278	8.489	8.275	8.142	7.084	A	M
26	75.539736	-70.417168	9.465	8.613	8.322	8.077	8.220	8.050	7.904	6.535	A	M
27	75.813714	-70.294932	9.782	8.985	8.715	8.637	8.725	8.536	8.424	7.530	A	M
28	76.020954	-70.379563	9.167	8.427	8.112	7.871	8.099	7.911	7.698	6.111	A	M
29	76.040897	-70.204907	9.465	8.676	8.390	8.207	8.408	8.191	8.096	7.963	A	M
30	76.058805	-67.270660	8.010	7.188	6.781	6.374	6.331	6.073	5.577	3.491	A	F
31	76.174095	-70.710382	9.184	8.380	8.029	7.817	7.893	7.619	7.371	5.406	A	M
32	76.225852	-70.555205	9.493	8.669	8.404	8.252	8.419	8.219	8.088	7.845	A	M
33	76.291645	-70.667688	9.429	8.647	8.383	8.215	8.365	8.170	8.094	7.850	A	M
34	76.389733	-70.563002	8.828	8.002	7.638	7.267	7.309	7.005	6.501	3.932	A	F
35	76.486300	-70.589963	9.234	8.440	8.114	7.791	7.860	7.542	7.113	4.957	A	M
36	76.495647	-70.487290	9.569	8.806	8.472	8.334	8.457	8.230	8.085	6.454	A	M
37	76.498117	-70.803169	9.483	8.715	8.315	7.691	7.711	7.405	6.914	4.507	A	P
38	76.651730	-70.544063	9.811	9.022	8.750	8.474	8.611	8.438	8.131	5.983	—	M
39	76.773682	-70.545627	8.123	7.383	7.044	6.793	6.931	6.710	6.472	4.886	A	M
40	76.885651	-70.651219	9.376	8.419	8.018	7.687	7.714	7.355	6.921	4.545	A	M
41	77.367843	-68.797713	10.045	9.095	8.658	8.270	8.143	7.937	7.657	6.415	M	F
42	77.431671	-65.366457	8.829	8.065	7.693	7.307	7.225	6.958	6.417	4.063	A	K
43	78.193212	-67.327190	8.783	7.982	7.590	7.223	7.013	6.683	6.098	3.602	A	F
44	78.707198	-67.455496	8.639	7.784	7.421	7.042	6.908	6.615	6.067	3.790	A	F
45	79.287434	-69.539210	9.015	8.163	7.824	7.517	7.444	7.177	6.615	4.223	A	M
46	79.484786	-69.673710	9.702	8.870	8.575	8.387	8.587	8.395	8.230	6.661	A	M

Table 1—Continued

No.	RA (°)	Decl (°)	J	H	K _S	[3.6]	[4.5]	[5.8]	[8.0]	[24]	Data ^a	Reference ^b
47	79.763600	-69.665335	8.530	7.913	7.604	7.379	7.332	7.027	6.510	4.586	A	M
48	79.972044	-69.459329	9.250	8.447	8.218	7.823	7.962	7.726	7.447	5.539	A	M
49	80.098385	-69.557466	9.080	8.329	7.983	7.766	7.711	7.427	6.882	4.330	A	M
50	80.366502	-69.504510	9.311	8.504	8.145	8.046	7.987	7.696	7.139	4.553	A	M
51	80.629539	-69.568088	9.784	8.963	8.649	—	8.510	8.209	7.793	6.997	A	M
52	80.761457	-69.343640	9.625	8.827	8.513	8.261	8.473	8.280	8.049	6.542	A	M
53	80.891611	-69.318588	—	—	—	—	8.851	8.737	—	8.144	A	M
54	80.931710	-65.699946	9.011	8.131	7.744	7.321	7.287	7.020	6.493	3.901	A	K
55	80.975513	-70.168343	10.039	9.119	8.774	8.741	8.674	8.431	8.140	6.578	M	M
56	81.080442	-69.647027	8.360	7.375	6.809	6.384	6.354	6.061	5.452	4.774	A M	K
57	81.436850	-69.080232	9.178	8.336	7.993	7.566	7.675	7.362	6.904	4.817	A	M
58	81.499584	-69.565144	11.718	10.961	10.731	10.597	10.426	10.257	—	—	M	F
59	81.547406	-66.203176	9.376	8.359	7.878	7.084	6.947	6.579	5.992	4.340	A M	K
60	81.567110	-66.116435	9.187	8.375	8.027	7.835	7.684	7.309	6.756	4.262	A M	K
61	81.614147	-69.182168	8.934	8.078	7.705	7.430	7.491	7.158	6.594	4.096	A	P
62	81.617605	-69.132679	9.606	8.759	8.483	8.246	8.450	8.237	8.011	6.352	A	M
63	81.645022	-68.861091	8.490	7.599	7.265	6.831	6.852	6.563	6.082	4.021	—	K
64	81.675405	-68.944066	9.696	8.817	8.550	8.330	8.537	8.255	8.099	7.029	A	M
65	81.678049	-68.953632	9.613	8.826	8.550	8.148	8.156	7.888	7.498	5.322	A	M
66	81.792519	-69.607455	10.399	9.544	9.159	8.942	8.829	8.501	8.232	6.99	M	M
67	81.792920	-69.271529	9.812	9.002	8.784	8.533	8.669	8.505	8.334	6.671	A	F
68	81.809231	-69.186349	9.355	8.551	8.192	7.870	7.893	7.607	7.303	5.246	A	M
69	81.861454	-69.521000	9.727	8.942	8.666	8.516	8.666	8.437	8.185	6.895	A	M
70	81.866884	-69.010018	9.405	8.592	8.323	8.187	—	7.988	7.679	6.021	A	M
71	81.873700	-67.236976	9.030	8.298	7.971	7.528	7.338	6.980	6.510	5.132	A	M
72	81.893100	-66.891674	8.942	8.206	7.837	7.343	7.418	7.123	6.601	4.316	A	P
73	81.915221	-69.150377	9.056	8.253	7.970	7.707	7.941	7.700	7.610	—	A	M
74	81.947921	-69.222399	8.815	7.998	7.604	7.275	7.282	6.857	6.103	4.030	A	K
75	81.962977	-67.301129	9.704	8.904	8.601	8.375	8.642	8.380	8.215	—	A	M
76	81.963061	-69.179399	9.445	8.626	8.288	8.100	8.263	8.075	8.030	7.680	A	M
77	82.024881	-69.120357	9.416	8.578	8.149	7.584	7.536	7.273	6.810	4.658	A	M
78	82.033607	-69.219738	9.185	8.360	8.001	7.739	7.689	7.458	6.977	4.555	A	M
79	82.064241	-66.981324	9.289	8.452	8.092	7.911	7.788	7.551	7.097	4.654	A	F
80	82.066198	-69.200268	9.625	8.800	8.514	8.281	8.579	8.360	8.308	8.043	A	M
81	82.077459	-69.126368	9.486	8.657	8.314	8.115	8.282	8.038	7.670	5.882	A	M
82	82.116319	-69.215940	8.974	8.666	8.384	—	7.934	7.739	7.431	5.968	A	M
83	82.120235	-68.118893	8.609	7.801	7.477	6.849	6.889	6.619	6.233	4.064	A	K
84	82.126448	-69.012338	9.653	8.772	8.503	8.393	8.429	8.203	7.919	6.424	A	M
85	82.131423	-69.091968	9.290	8.396	8.049	7.802	7.932	7.652	7.319	5.186	A	M
86	82.177000	-69.128438	9.988	9.286	8.995	8.613	8.623	8.358	7.924	5.869	—	M
87	82.179938	-67.307893	9.613	8.822	8.582	8.327	8.573	8.308	8.086	7.572	A	M
88	82.189510	-68.967304	8.710	7.941	7.549	7.295	7.464	7.185	6.847	5.339	A	M
89	82.215933	-70.012402	10.244	9.346	8.980	8.712	8.574	8.333	8.047	6.712	M	F
90	82.249936	-67.750382	11.482	10.556	10.066	9.889	9.973	9.724	9.522	9.194	M	F
91	82.253219	-68.775960	9.557	8.739	8.435	8.188	8.286	8.008	7.635	5.771	A	M
92	82.264496	-69.112835	9.095	8.263	7.901	7.494	7.441	7.168	6.633	3.927	A	F

Table 1—Continued

No.	RA (°)	Decl (°)	J	H	K _S	[3.6]	[4.5]	[5.8]	[8.0]	[24]	Data ^a	Reference ^b
93	82.272933	-67.304874	9.695	8.847	8.574	8.466	8.615	8.442	8.307	—	A	M
94	82.285018	-69.205096	9.458	8.668	8.345	8.084	8.259	8.016	7.698	5.576	A	M
95	82.337464	-68.792041	8.954	8.248	7.974	7.809	7.935	7.669	7.416	6.762	A	M
96	82.339290	-69.005629	8.833	8.033	7.746	7.340	7.437	7.052	6.572	4.826	A	M
97	82.364952	-69.147313	8.407	7.675	7.303	6.756	6.817	6.463	5.920	3.938	A	K
98	82.393450	-66.924538	9.846	9.051	8.730	—	7.800	7.490	6.812	4.418	A M	F
99	82.425819	-68.954832	7.922	7.192	6.886	6.657	6.774	6.534	6.168	4.444	A	M
100	82.433175	-69.097210	8.989	8.180	7.882	7.563	7.536	7.288	6.940	4.934	A	M
101	82.478150	-69.071027	9.420	8.688	8.406	8.215	8.364	8.138	7.881	6.804	A	M
102	82.478929	-67.310215	8.900	8.124	7.789	7.356	7.374	7.029	6.456	4.305	A	M
103	82.509512	-67.045854	8.755	8.162	7.974	7.672	7.734	7.513	7.282	5.983	A	M
104	82.519134	-68.791330	9.804	9.032	8.769	8.574	8.801	8.596	8.401	7.408	A	M
105	82.520562	-69.066599	9.900	9.075	8.808	8.590	8.781	8.546	8.269	6.879	A	M
106	82.539901	-69.184357	9.839	8.942	8.641	8.391	8.619	8.402	8.261	7.403	A	M
107	82.587314	-67.334840	8.448	7.783	7.452	7.022	6.797	6.444	5.753	3.786	A	K
108	82.592061	-67.108752	9.697	8.932	8.603	8.438	8.589	8.441	8.318	7.078	A	M
109	82.609471	-69.506780	9.598	8.822	8.478	8.285	8.432	8.187	7.880	5.763	A	M
110	82.639484	-67.287532	9.215	8.393	8.121	7.998	8.089	7.934	7.810	7.778	A	M
111	82.648062	-68.989827	8.747	7.897	7.553	7.184	7.283	7.024	6.625	4.347	A	P
112	82.648212	-67.201204	9.913	9.159	8.852	8.726	8.868	8.720	8.535	7.647	A	M
113	82.672671	-69.259404	8.752	7.993	7.591	7.549	7.375	7.108	6.614	4.179	A	F
114	82.674892	-69.089771	9.889	9.079	8.756	8.464	8.630	8.381	8.040	6.263	A	M
115	82.688204	-67.133163	9.598	8.781	8.431	8.174	8.402	8.148	7.966	6.493	A	M
116	82.717866	-67.292882	9.865	9.040	8.827	8.618	8.726	8.566	8.390	6.802	A	M
117	82.751940	-69.177779	10.728	9.849	9.554	9.298	9.467	9.283	9.284	—	A	M
118	82.755027	-69.183132	9.480	8.623	8.328	8.020	8.100	7.739	7.223	5.228	A	M
119	82.764302	-69.094463	9.621	8.787	8.582	8.375	8.513	8.366	8.333	8.341	A	M
120	82.767398	-69.317501	9.022	8.060	7.627	6.981	6.901	6.519	5.899	4.181	A	K
121	82.788629	-67.431940	8.797	7.948	7.631	7.394	7.505	7.286	7.064	5.221	A	M
122	82.814424	-69.066357	9.394	8.524	8.219	7.919	8.027	7.741	7.237	5.793	A	M
123	82.826852	-69.157832	9.778	8.954	8.628	8.434	8.496	8.352	8.237	8.145	A	M
124	82.903446	-66.502146	8.476	7.728	7.374	6.924	6.945	6.663	6.225	4.050	A	K
125	82.947519	-67.384246	9.594	8.842	8.588	8.350	8.468	8.231	7.990	6.182	A	M
126	83.036714	-67.188513	9.764	8.975	8.692	8.405	8.600	8.408	8.198	6.941	A	M
127	83.080233	-67.416724	9.914	9.144	8.874	8.692	8.839	8.734	8.607	8.187	A	M
128	83.114295	-69.281282	9.075	8.261	7.963	7.766	7.858	7.595	7.228	5.059	A	M
129	83.130593	-69.340385	9.744	8.901	8.630	—	8.670	8.420	8.286	7.454	A	M
130	83.147117	-69.131018	9.466	8.575	8.263	7.975	7.981	7.817	7.532	5.594	A	M
131	83.209336	-67.462504	9.179	8.331	8.048	7.734	7.931	7.581	7.142	5.483	A	M
132	83.281690	-66.801580	9.781	9.042	8.614	7.808	7.585	7.167	6.363	4.317	A M	P
133	83.310319	-67.063479	9.432	8.587	8.320	8.051	8.283	8.045	7.919	6.442	A	M
134	83.361725	-67.070424	8.953	8.195	7.818	7.300	7.210	6.823	6.142	3.979	A	K
135	83.373315	-67.527127	9.949	9.151	8.825	8.682	8.790	8.656	8.589	8.117	A	M
136	83.435633	-67.404693	9.705	8.843	8.489	8.148	8.162	7.824	7.269	5.621	A M	M
137	83.467379	-69.187088	9.220	8.356	7.899	7.440	7.401	7.090	6.624	4.320	A	M
138	83.558570	-68.978860	9.272	8.370	7.956	7.574	7.313	6.996	6.461	3.918	A M	F

Table 1—Continued

No.	RA (°)	Decl (°)	J	H	K _S	[3.6]	[4.5]	[5.8]	[8.0]	[24]	Data ^a	Reference ^b
139	83.581189	-68.993541	9.634	8.822	8.533	8.349	8.493	8.250	7.967	6.029	A	M
140	83.589252	-69.366740	9.912	9.113	8.891	8.775	8.704	8.589	8.502	8.413	A	M
141	83.640732	-69.250679	9.465	8.580	8.278	8.017	8.200	8.003	7.718	5.776	A	M
142	83.695939	-69.483476	10.068	9.275	9.020	8.867	8.996	8.877	8.791	8.714	A	M
143	83.808775	-67.732191	9.376	8.533	8.024	7.379	7.171	6.840	6.293	3.813	A	F
144	83.828775	-67.038816	9.541	8.706	8.336	7.970	8.084	7.783	7.373	4.902	A	P
145	83.852212	-69.067616	9.567	8.657	8.234	7.785	7.801	7.495	7.056	4.854	A M	M
146	83.867980	-66.934027	8.359	7.579	7.259	7.050	7.025	6.771	6.251	4.035	A	K
147	83.886724	-69.071993	9.449	8.567	8.197	7.934	8.105	7.909	7.791	—	A	M
148	83.932594	-68.855835	9.121	8.270	8.044	7.690	7.829	7.511	7.051	5.358	A	M
149	83.966537	-69.374751	9.567	8.706	8.451	8.271	8.440	8.263	8.202	8.140	A	M
150	83.980150	-69.166502	8.543	7.632	7.135	6.820	6.759	6.324	5.612	3.712	A	K
151	84.026578	-68.944660	9.548	8.738	8.442	8.168	8.370	8.195	8.066	7.807	A	M
152	84.044369	-68.911174	9.164	8.319	7.968	7.453	7.531	7.161	6.554	4.423	A	M
153	84.084997	-68.938532	9.704	8.743	8.354	7.840	7.931	7.426	6.890	5.271	A M	M
154	84.106074	-66.927346	8.638	7.888	7.496	7.033	6.971	6.712	6.226	3.647	A	F
155	84.111546	-69.397579	8.482	8.039	7.811	7.611	7.624	7.218	6.614	3.735	A	M
156	84.169085	-69.387874	9.872	9.061	8.812	8.499	8.544	8.268	7.897	6.547	A	M
157	84.335449	-69.327410	9.418	8.541	8.278	8.049	8.156	7.939	7.630	6.572	A	M
158	84.359859	-68.794516	9.406	8.576	8.226	7.976	8.105	7.863	7.654	5.904	A	M
159	84.377738	-69.042524	9.928	9.057	8.721	8.450	8.561	8.361	8.138	7.012	A	M
160	84.403673	-69.489890	9.455	8.560	8.211	8.028	8.055	7.830	7.345	4.853	A	M
161	84.429627	-69.416735	9.058	8.188	7.871	7.626	7.776	7.473	6.969	—	A	M
162	84.437941	-69.346846	8.961	8.177	7.715	7.250	7.054	6.687	6.081	3.612	A	K
163	84.494492	-69.239996	9.532	8.716	8.383	7.969	7.986	7.781	7.590	7.336	A	M
164	84.527712	-69.291588	9.339	8.395	7.913	7.489	7.610	7.283	6.889	4.861	A	M
165	84.566732	-69.169779	9.308	8.336	7.867	7.498	7.283	6.925	6.281	4.102	—	M
166	84.575514	-69.295149	9.607	8.647	8.304	7.994	8.127	7.733	7.379	5.490	A	M
167	84.641794	-69.342182	10.211	9.379	8.508	7.251	6.276	5.559	4.371	—	A	K
168	84.942562	-69.324538	9.698	8.761	8.473	8.193	8.390	8.105	7.694	5.701	A	M
169	84.987101	-69.589185	10.759	9.900	9.589	9.540	9.361	9.138	8.966	—	M	F
170	85.032042	-69.334746	9.481	8.610	8.286	8.054	8.089	7.831	7.459	5.114	—	M
171	85.070984	-69.465015	9.373	8.487	8.220	7.995	7.985	7.675	7.262	5.041	A	M
172	85.102157	-69.354771	9.140	8.259	7.854	7.539	7.560	7.244	6.755	4.555	A	M
173	85.105752	-69.258410	9.774	9.073	8.783	8.525	8.354	8.079	7.655	5.874	A	M
174	85.154144	-69.439026	9.494	8.674	8.322	8.034	8.097	7.775	7.337	5.392	A	M
175	85.182553	-69.366179	8.819	7.909	7.445	7.054	7.059	6.670	6.138	4.664	A	M
176	85.202334	-69.560030	9.165	8.201	7.711	7.098	6.937	6.552	5.839	3.493	A	K
177	85.230778	-69.390385	8.827	7.873	7.544	7.248	7.392	7.128	6.824	4.971	A	M
178	85.246957	-69.310076	—	—	—	7.013	6.925	6.652	7.307	3.685	A	M
179	85.271164	-69.078427	9.230	8.319	7.975	7.820	7.976	7.723	7.488	5.761	A	M
180	85.278948	-69.287421	8.956	8.170	7.772	7.283	7.397	7.114	6.811	4.617	A	M
181	85.294802	-69.634524	8.789	7.982	7.631	—	7.274	6.951	6.602	4.559	A	K
182	85.340759	-69.530296	8.996	8.163	7.818	7.549	7.578	7.302	6.898	—	A	M
183	85.373065	-69.454438	9.589	8.727	8.452	8.249	8.400	8.208	8.024	7.515	A	M
184	85.430854	-69.470982	9.520	8.716	8.412	8.172	8.275	8.061	7.730	—	A	M

Table 1—Continued

No.	RA (°)	Decl (°)	J	H	K _S	[3.6]	[4.5]	[5.8]	[8.0]	[24]	Data ^a	Reference ^b
185	85.433494	-69.200771	9.579	8.704	8.400	8.122	8.348	8.107	7.912	6.661	A	M
186	85.458991	-69.354324	9.599	8.788	8.560	8.335	8.488	8.293	8.066	6.477	A	M
187	85.503057	-69.193601	9.900	9.017	8.683	8.390	8.586	8.345	8.048	6.661	—	M
188	85.660761	-69.164291	9.930	9.119	8.816	8.642	8.703	8.455	8.142	6.415	A	M
189	85.758491	-69.097160	9.502	8.637	8.366	8.172	8.261	8.129	8.018	—	A	M
190	87.305605	-70.711291	10.823	10.019	9.445	8.567	8.281	8.060	7.730	6.568	M	F
191	88.116003	-69.236126	10.605	9.754	9.204	8.451	8.221	8.062	7.860	7.093	M	F

^aPhotometry data resource: 'A' for ASAS, 'M' for MACHO and '—' for null.

^bReference: 'F' for Feast et al. (1980), 'P' for Pierce et al. (2000), 'M' for Massey & Olsen (2003), 'K' for Kastner et al. (2008)

Table 2. Results of the visual light variation by the PDM and Period04 methods for the 47 semi-regular and LSP RSGs with distinguishable short period

No.	$\langle m_V \rangle$	PDM			Period04		Measurements
		Period (d)	Amplitude (mag)	Theta	Period (d)	Amplitude (mag)	
9	10.87	634	0.18	0.51	625	0.07	478
10	12.94	810	0.55	0.49	800	0.20	532
11	12.98	420	0.73	0.68	431	0.24	440
13	13.05	976	0.48	0.45	943	0.17	254
14	12.62	680	0.67	0.41	645	0.27	529
15	13.22	668	0.55	0.34	680	0.24	337
16	12.00	656	0.50	0.43	653	0.22	500
17	12.22	657	0.49	0.40	662	0.20	511
24	13.13	873	0.86	0.30	869	0.60	493
28	12.56	407	0.29	0.51	425	0.08	518
30	12.36	1012	1.03	0.29	990	0.68	585
34	12.90	676	0.60	0.21	684	0.32	513
37	13.20	512	0.74	0.41	518	0.38	549
39	11.65	676	0.36	0.45	684	0.14	561
40	13.44	452	0.68	0.60	450	0.23	544
42	12.77	656	0.93	0.42	645	0.48	510
43	12.45	734	0.80	0.14	735	0.49	520
44	12.72	827	1.26	0.12	833	0.83	817
59	14.81	647	1.63	0.49	625	0.25	296
72	13.15	571	1.20	0.41	571	0.66	888
78	13.37	524	1.00	0.57	500	0.35	508
79	13.00	562	0.75	0.50	555	0.27	981
83	12.40	715	0.77	0.39	704	0.31	816
92	13.97	720	0.80	0.44	694	0.33	396
95	11.94	445	0.47	0.50	446	0.22	934
97	12.18	684	0.75	0.30	689	0.34	624
99	11.47	761	0.50	0.26	763	0.28	769
101	12.05	314	0.29	0.58	311	0.08	686
102	12.48	628	0.51	0.56	598	0.13	1275
103	11.41	505	0.42	0.51	515	0.14	1208
107	12.37	684	0.89	0.42	666	0.28	1156
111	13.10	487	0.64	0.61	478	0.20	736
113	12.32	671	0.74	0.32	675	0.44	415
121	13.06	599	0.77	0.33	606	0.33	1107
124	12.05	766	0.70	0.19	751	0.42	1011
132	14.17	447	3.33	0.43	403	0.14	316
134	12.68	531	0.66	0.53	537	0.25	1017
136	13.29	399	0.81	0.54	401	0.14	332
146	11.65	689	0.37	0.32	735	0.11	759
150	11.21	675	0.09	0.48	689	0.04	407
157	11.38	389	0.14	0.53	393	0.04	600
162	11.63	730	0.26	0.42	699	0.09	672
175	13.75	630	0.75	0.50	636	0.22	437
177	13.30	544	1.17	0.54	549	0.26	509
180	13.02	555	0.80	0.63	543	0.21	567

Table 2—Continued

No.	$\langle m_V \rangle$	PDM			Period04		Measurements
		Period (d)	Amplitude (mag)	Theta	Period (d)	Amplitude (mag)	
182	12.71	586	0.34	0.68	584	0.13	566
186	13.10	275	0.30	0.63	280	0.07	574

Table 3. Results of the fitted linear P-L relations for the 47 Semi-regular RSGs and LSP RSGs with distinguishable short period

Band	Slope a	intercept b	χ^2
V	-1.97 ± 1.03	18.13 ± 2.85	0.81
J	-3.61 ± 0.38	18.91 ± 1.06	0.32
H	-3.58 ± 0.34	18.02 ± 0.95	0.29
K_S	-3.75 ± 0.32	18.13 ± 0.88	0.26
[3.6]	-3.98 ± 0.29	18.40 ± 0.80	0.24
[4.5]	-4.35 ± 0.25	19.41 ± 0.68	0.20
[5.8]	-4.54 ± 0.28	19.65 ± 0.79	0.23
[8.0]	-5.34 ± 0.39	21.43 ± 1.10	0.32
[24]	-7.83 ± 0.75	26.34 ± 2.14	0.59

Table 4. The period and amplitude of the 51 LSP RSGs

No.	Period (d)	Amplitude (mag)
3	2087	0.23
7	2164	0.07
20	2710	0.08
22	2304	0.03
25	2457	0.20
27	2544	0.11
33	1897	0.05
35	1661	0.34
46	2252	0.08
48	2364	0.15
53	1175	0.06
64	2976	0.03
69	2092	0.10
73	2364	0.09
74	2444	0.17
75	1893	0.07
76	2481	0.23
80	1597	0.08
84	2421	0.12
87	2680	0.14
93	1715	0.08
96	2570	0.07
100	1587	0.06
102	2298	0.23
104	1342	0.05
105	2557	0.07
106	1579	0.09
108	2762	0.05
114	2958	0.16
115	1663	0.06
120	2433	0.16
122	2155	0.16
125	1248	0.06
126	1841	0.10
127	1811	0.06
128	1470	0.13
129	2314	0.08
131	2873	0.09
133	2816	0.17
135	2915	0.09
147	2040	0.08
148	2481	0.13
152	2976	0.05
160	2252	0.17
161	2832	0.15
166	902	0.09

Table 4—Continued

No.	Period (d)	Amplitude (mag)
172	2754	0.23
177	2232	0.28
183	1782	0.04
184	2624	0.13
189	1879	0.12

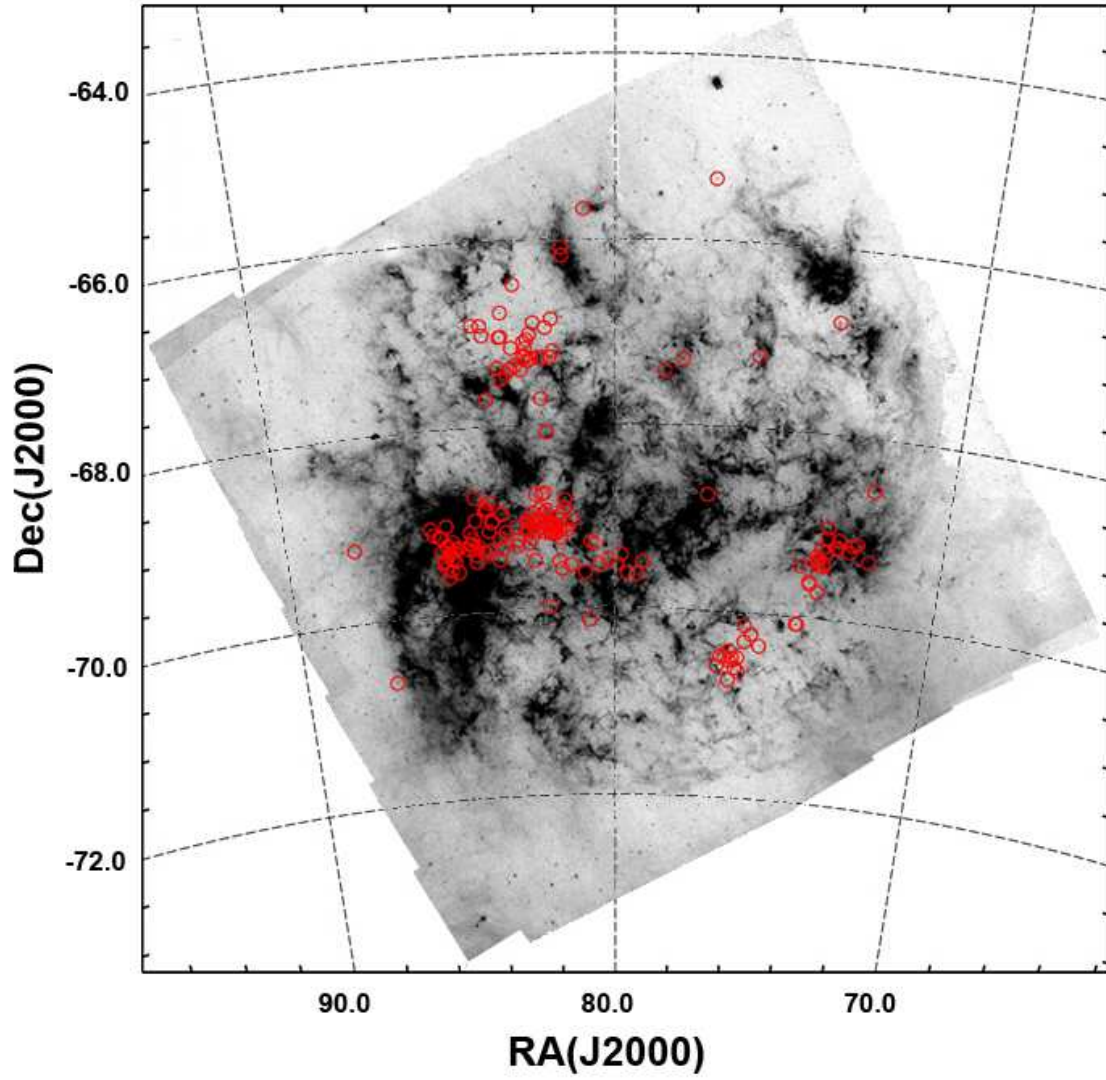


Fig. 1.— The spatial distribution of all the 191 sample stars superposed on the *Spitzer*/SAGE $8\mu\text{m}$ mosaic image. Many stars clump near the 30 Doradus area.

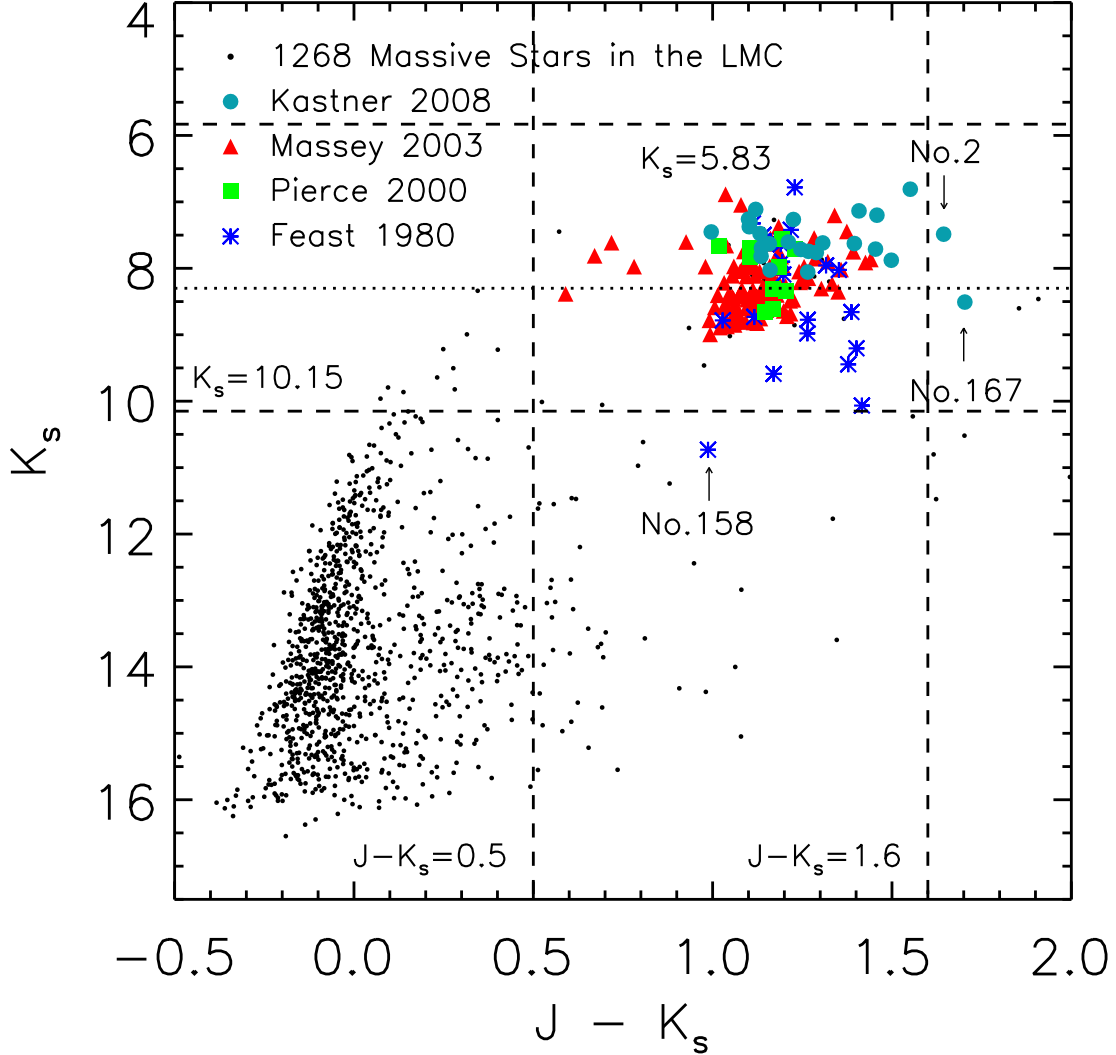


Fig. 2.— $[K_S]$ vs. $J - [K_S]$ CMD for all targets. For comparison, the 1268 massive stars from Bonanos et al. (2009) are added as background and denoted by black dots. Different symbols represent different resources. Most of the targets clump at $J - K_S = 0.5 \sim 1.6$. The vertical dashed line with $J - K_S = 1.6$ gives the boundary of carbon-rich star (Hughes & Wood 1990) and another with $J - K_S = 0.5$ the observational boundary of RSGs in LMC (Josselin et al. 2000). The horizontal dashed lines with $K_S = 5.83$ and $K_S = 10.15$ show the theoretical luminosity boundaries in the K_S band (see the text for details). The dotted line shows the criterion of $M_{\text{bol}} = -7.1$ to distinguish the AGB and RSG stars defined by Wood et al. (1983).

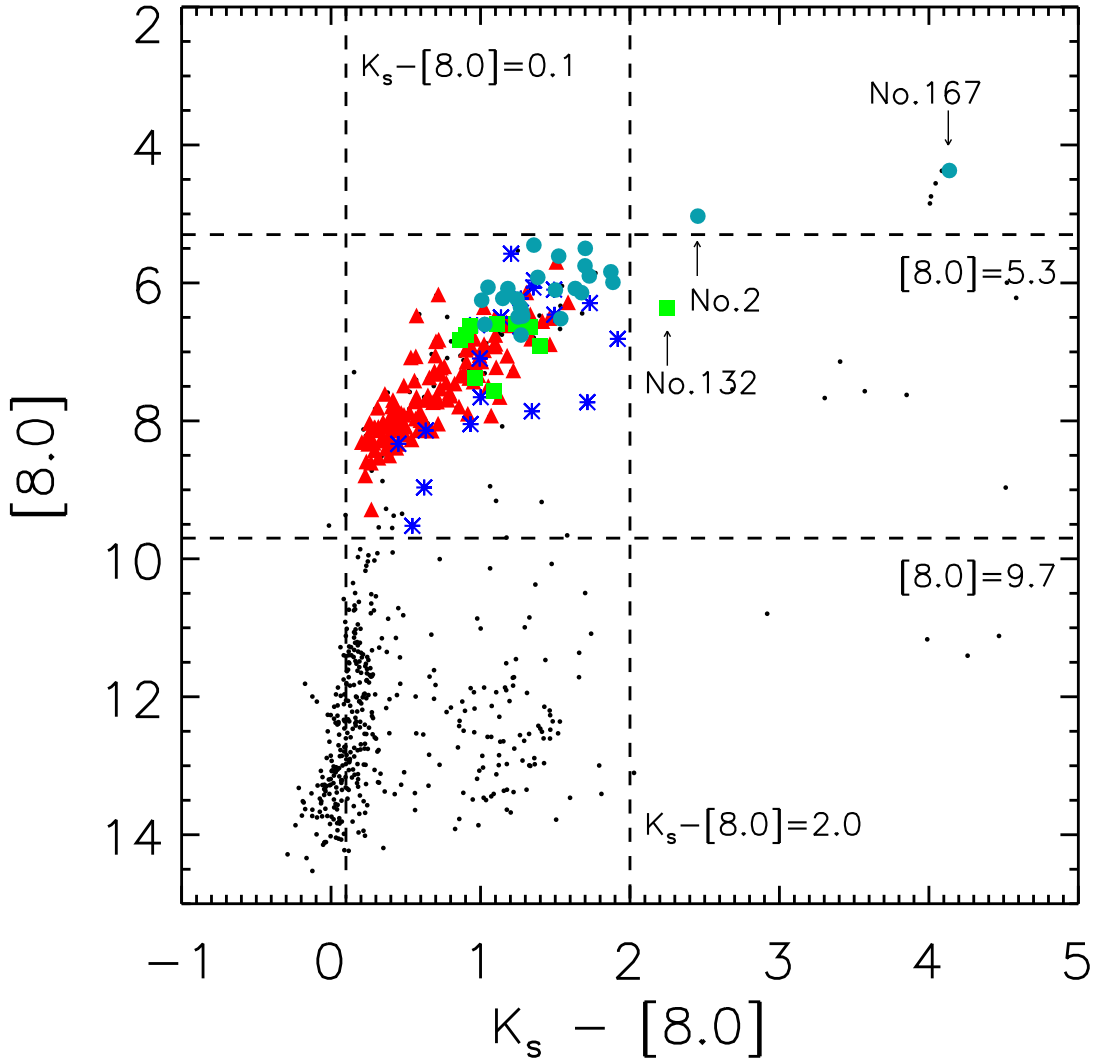


Fig. 3.— The same as Fig. 2, but for $[8.0]$ vs. $K_s - [8.0]$. We set our own limits for RSGs to include 98% clumped targets: $5.3 \leq [8.0] \leq 9.7$ and $0.1 \leq K_s - [8.0] \leq 2.0$.

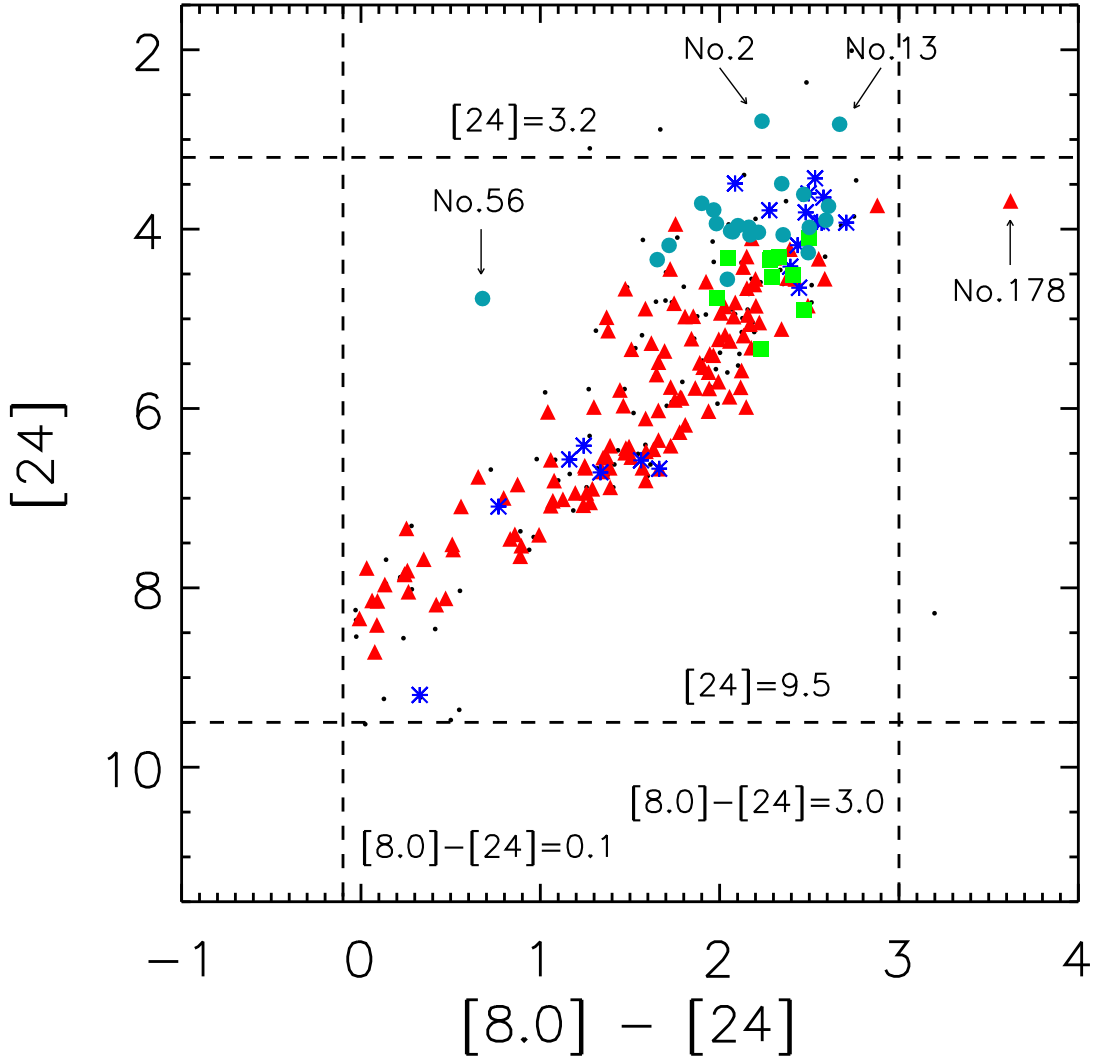


Fig. 4.— The same as Fig. 2, but for [24] vs. [8.0] - [24]. We also give the empirical limits for RSGs as $3.2 \leq [24] \leq 9.5$ and $-0.1 \leq [8.0] - [24] \leq 3.0$.

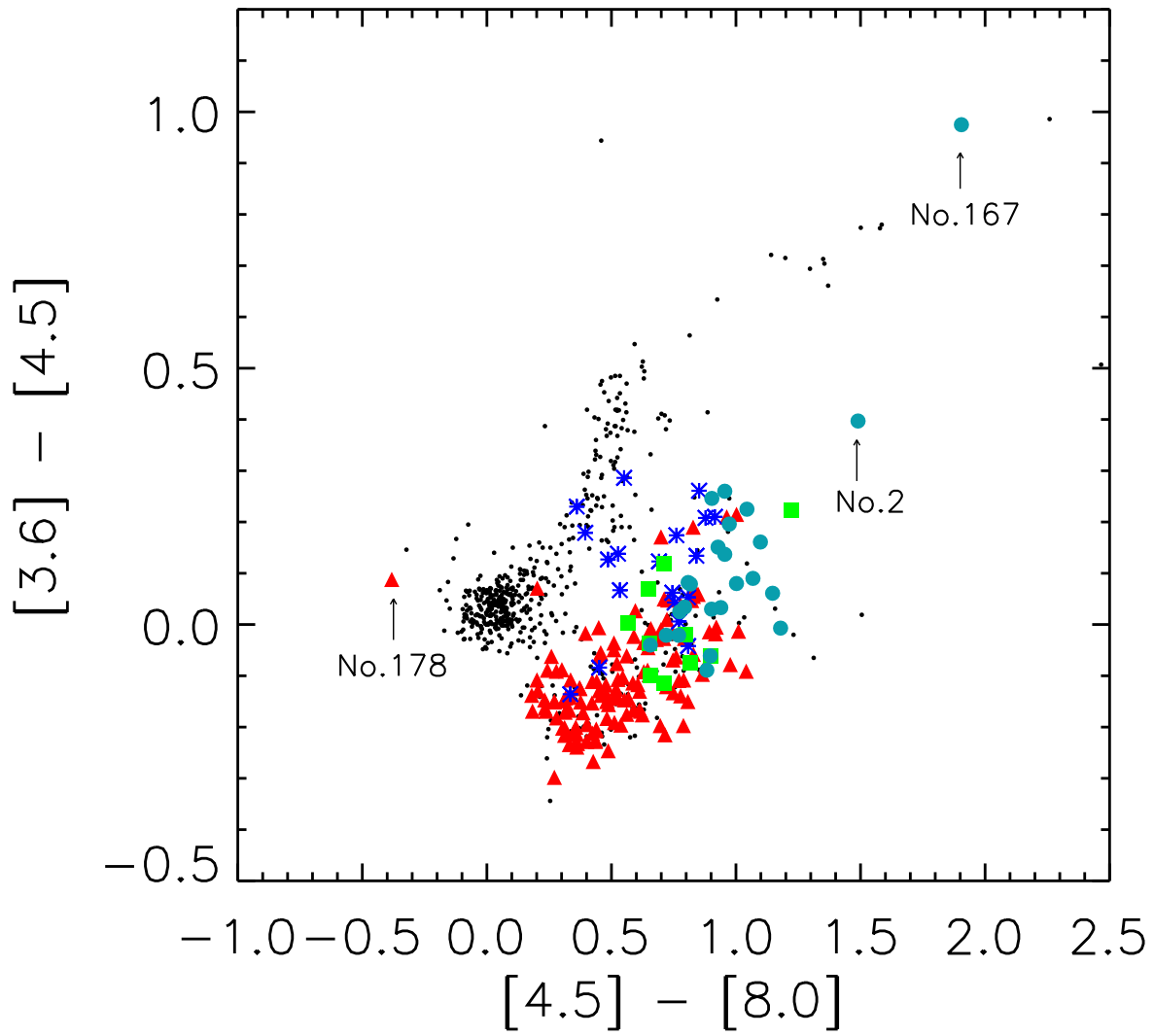


Fig. 5.— The color-color diagram $[3.6] - [4.5]$ vs. $[4.5] - [8.0]$. The symbols have the same meaning as in Fig. 2.

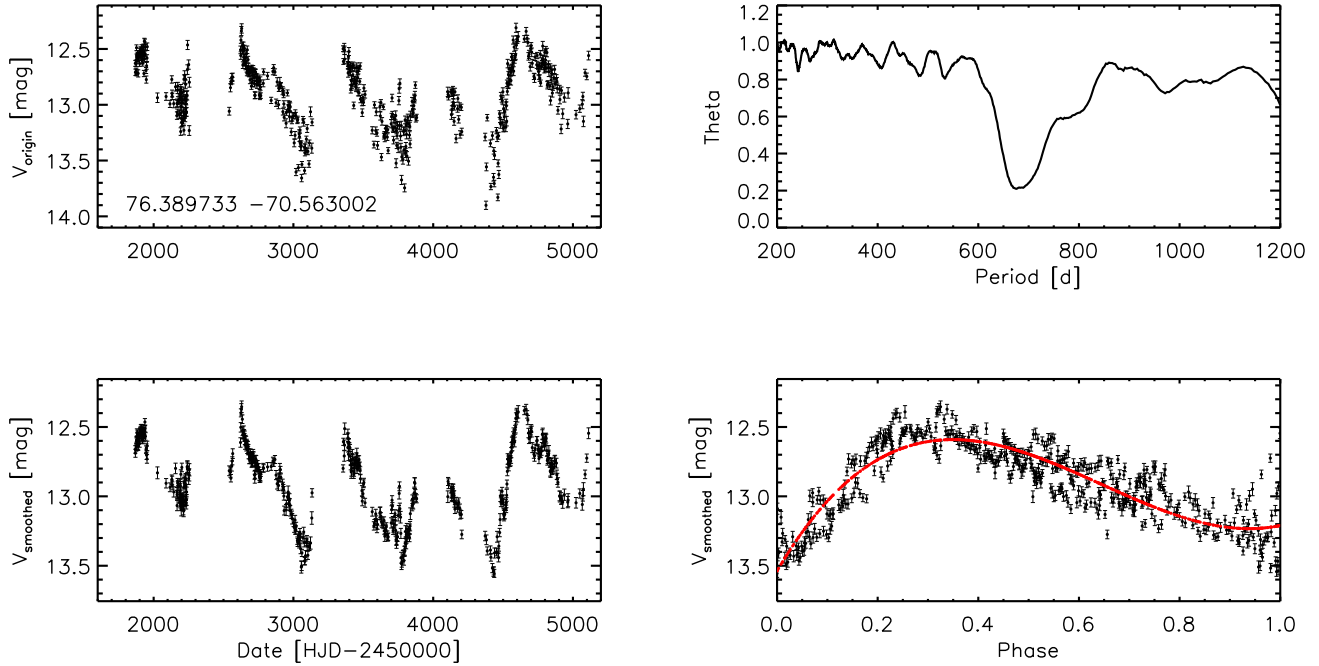


Fig. 6.— An example to show the PDM processing of the ASAS data for the star No.34 in Table 1. Left column from top to bottom: original light curve, smoothed light curve; right column from top to bottom: theta diagram, phase diagram. The coordinates are shown inside the top panel of left column. The red line shows the robust polynomial fitting curve.

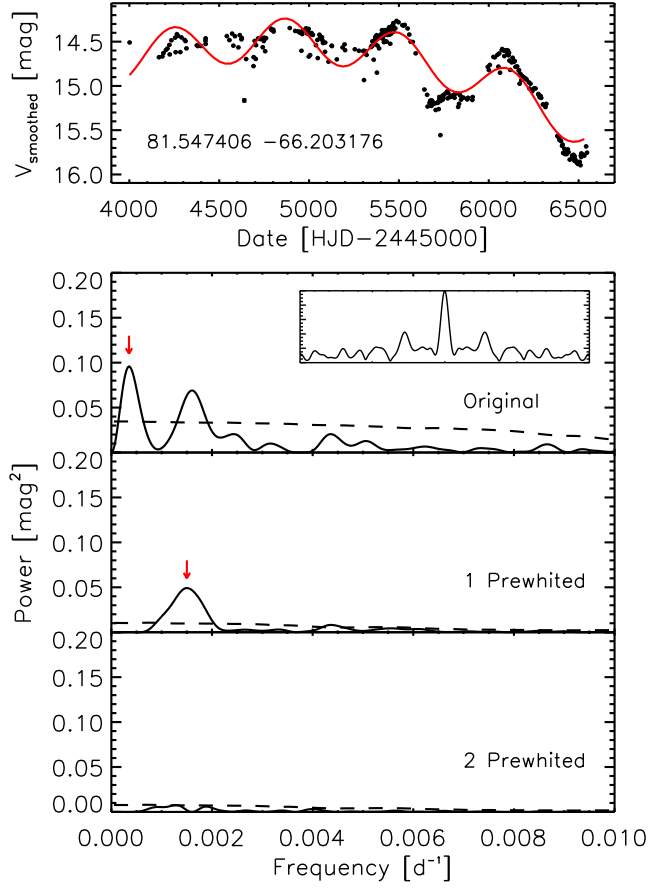


Fig. 7.— An example to show the Period04 processing of the MACHO data for the star No.59 in Table 1. Top panel is the original light curve with red fitting curve; bottom panel is the power spectra. The coordinates are shown inside the top panel. The spectral window in the first power spectrum diagram is shown in the same scale as the power spectra. The dashed line shows the four times noise spectrum. The red arrow marks the highest peak in the power spectra during each iteration.

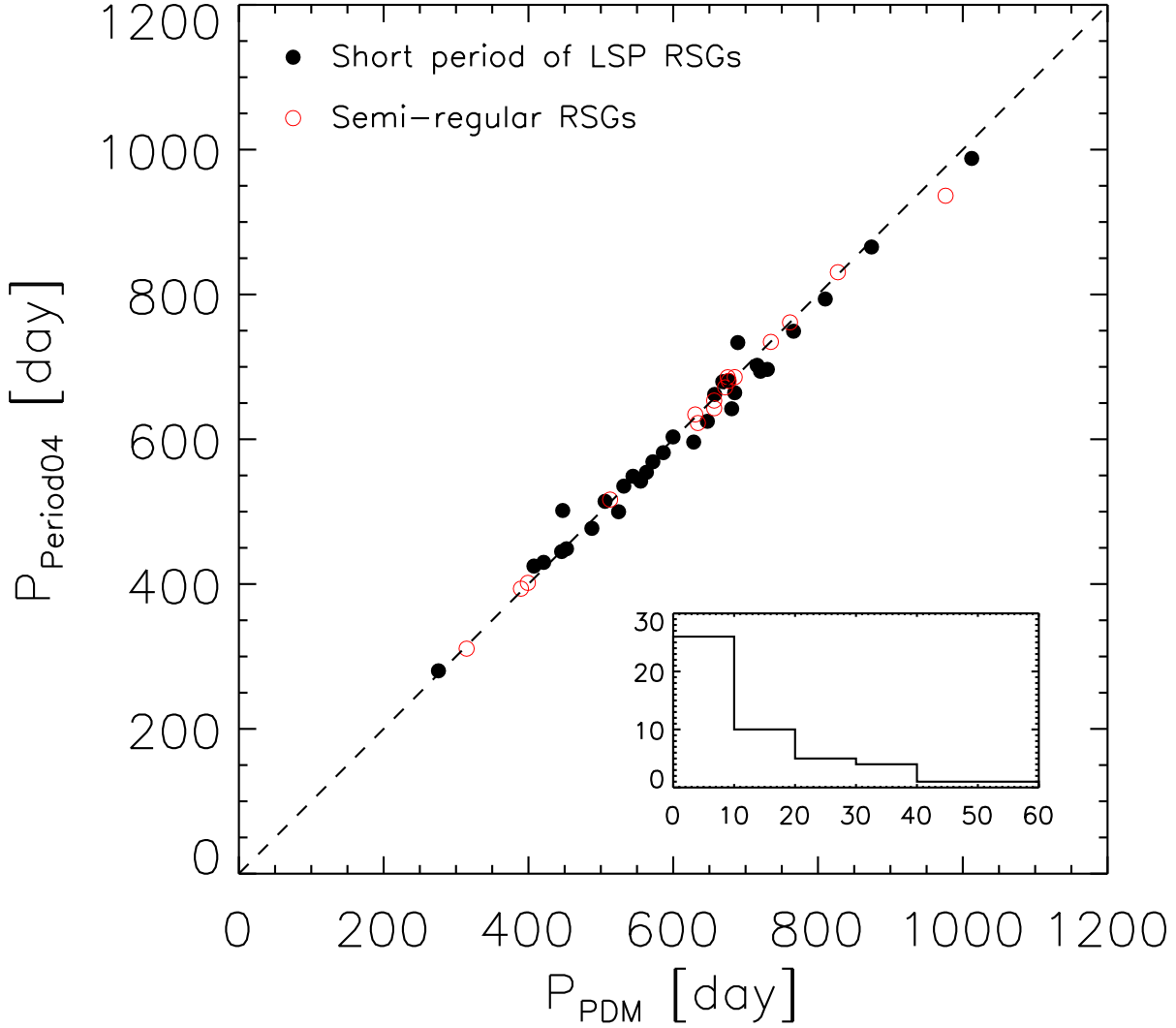


Fig. 8.— A comparison of the periods derived from the PDM and Period04 method respectively for the 47 semi-regular RSGs and Distinguishable Short Period LSP RSGs. The open red circles indicate the only one period of semi-regular RSGs and the filled black circles indicate the distinguishable short period of LSP RSGs which have both LSP and short period. The inset histogram shows the distribution of the difference between these two methods.

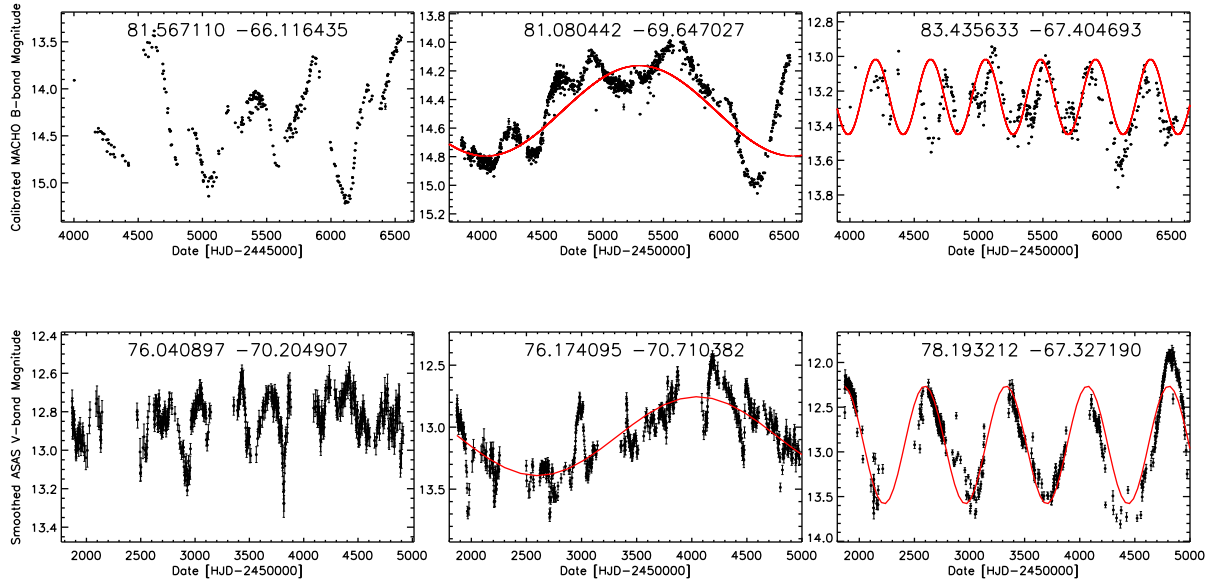


Fig. 9.— The sample light curves of three types of variation. From left to right: irregular light curve, long secondary period light curve and semi-regular light curve. Top panel: the ASAS data, bottom panel: the MACHO data. In each diagram, the coordinates are shown in the top. Red line shows the fitted curve.

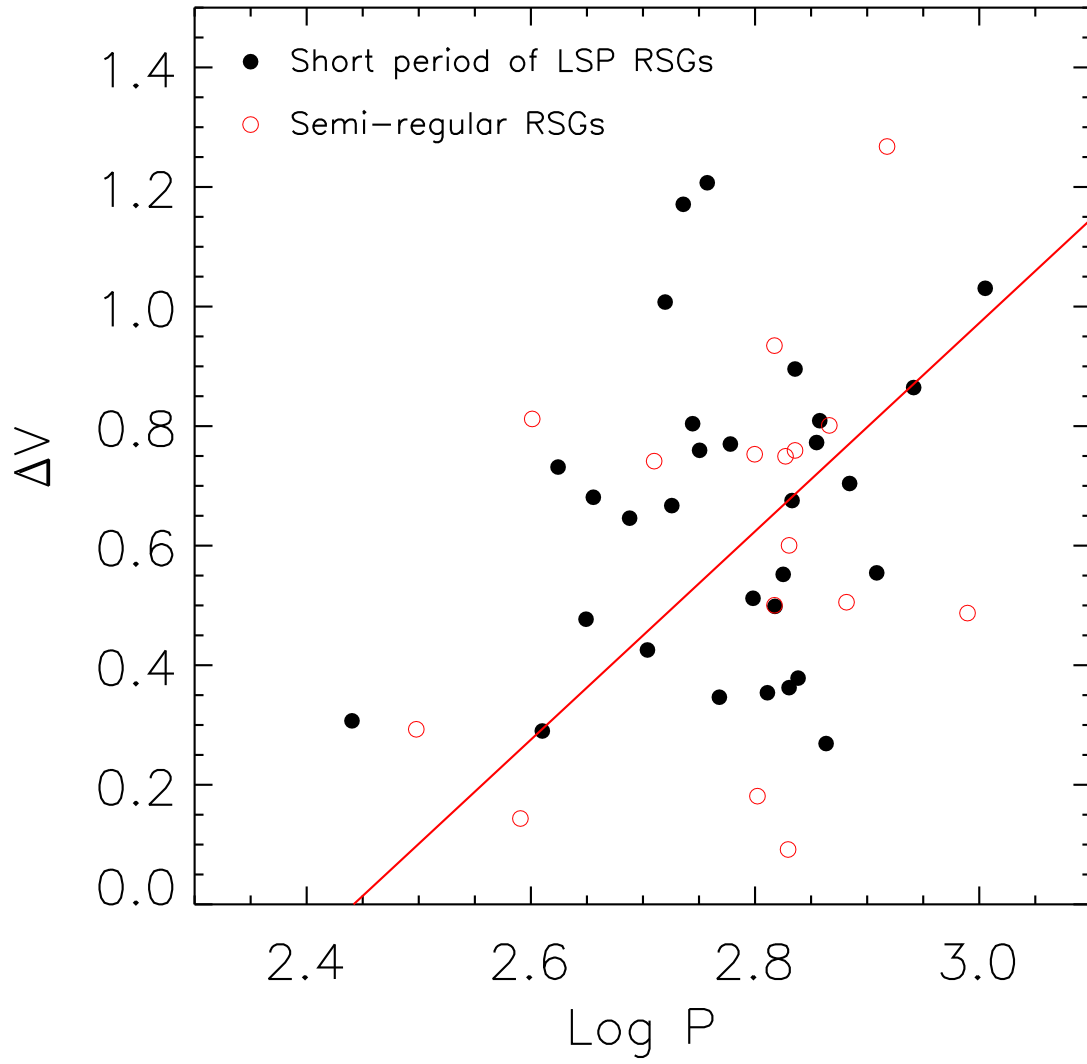


Fig. 10.— The period and the full amplitude of the 47 semi-regular RSGs and LSP RSGs with distinguishable short period. The red solid line is a linear fit between the amplitude and the period.

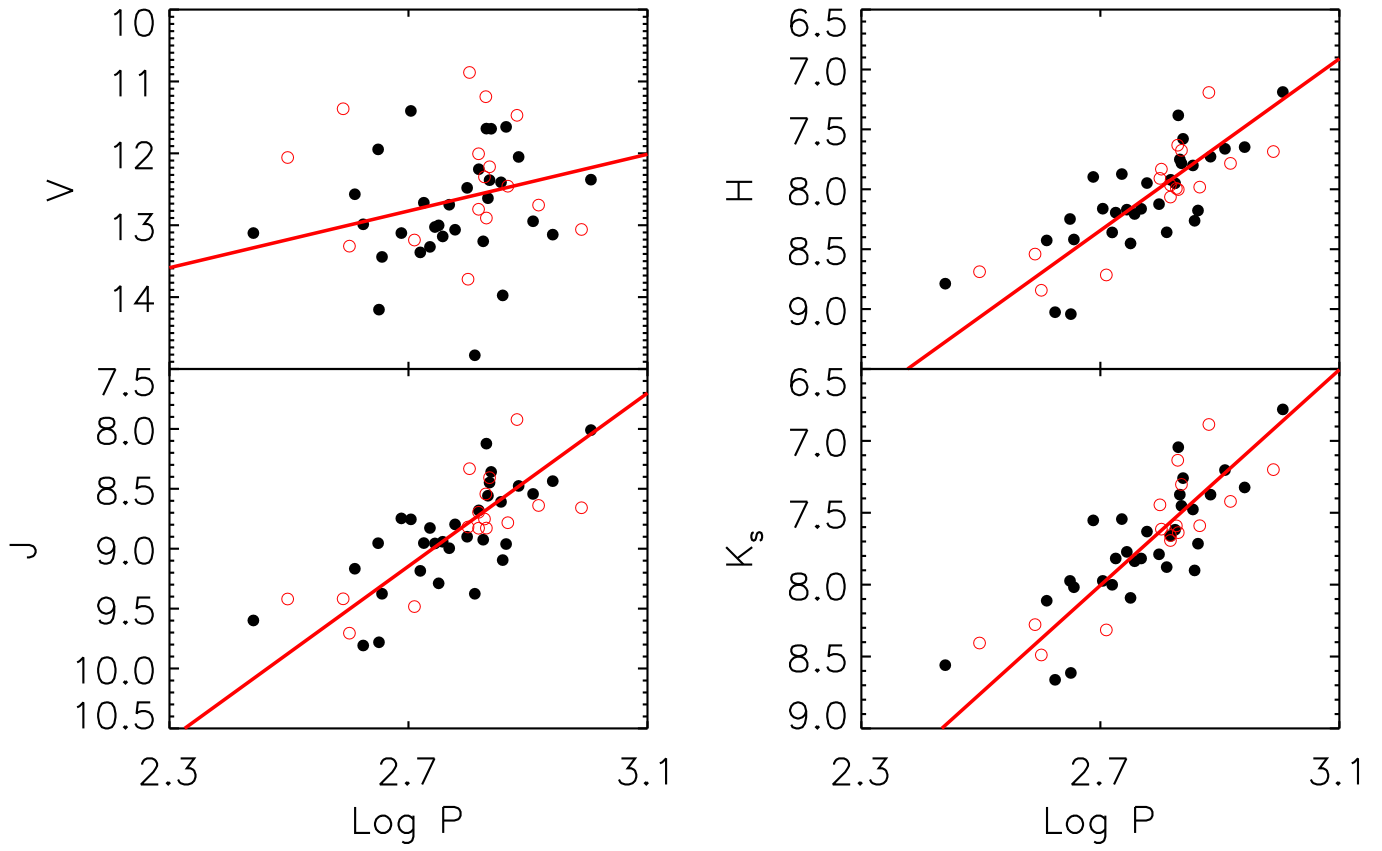


Fig. 11.— The Period-Luminosity relation in the V, J, H, and K_s bands for the 47 semi-regular RSGs and LSP RSGs with distinguishable short period. The symbols are the same as in Fig. 10.

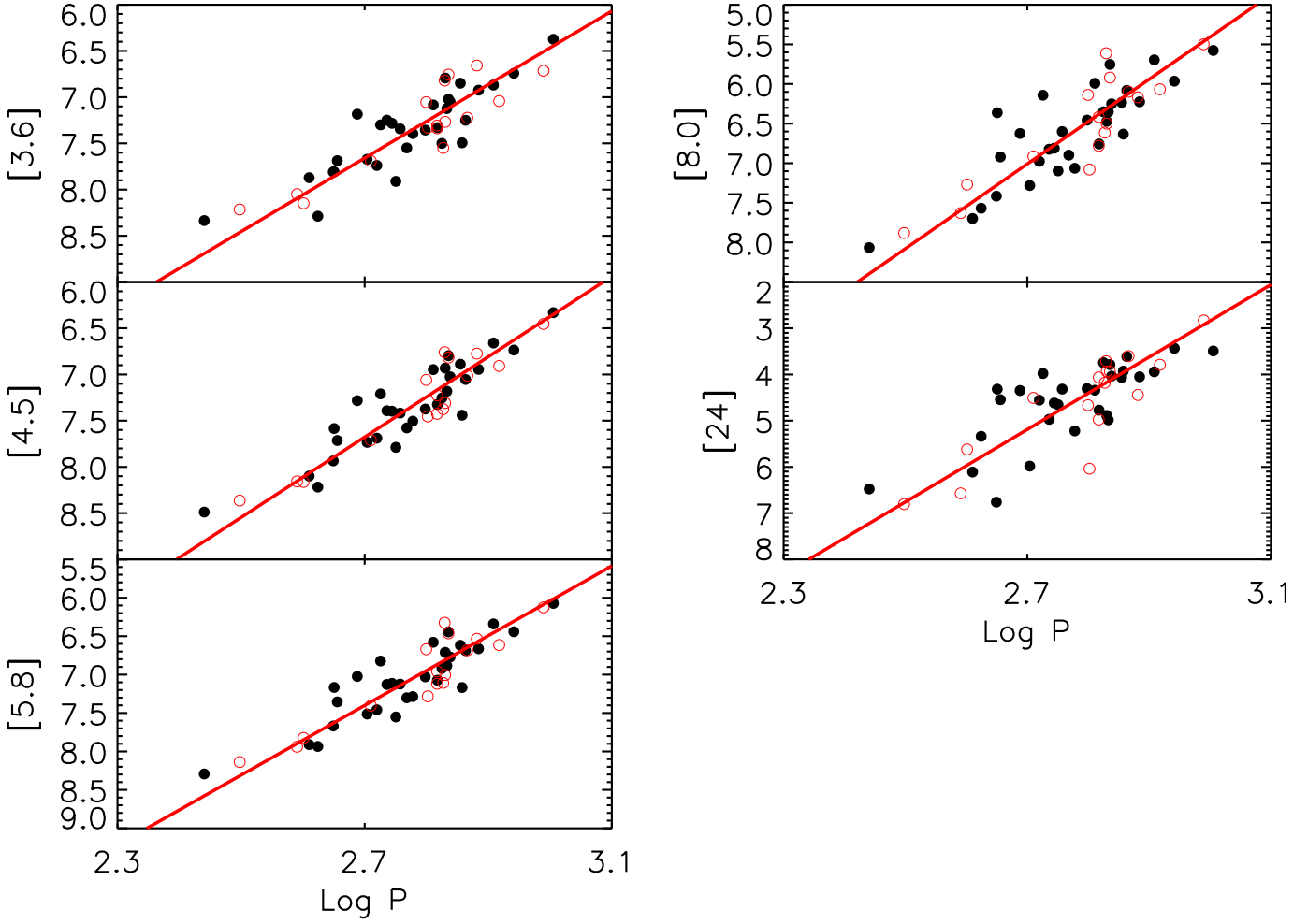


Fig. 12.— The same as Fig. 11, but the P-L relation is in the *Spitzer*/IRAC [3.6], [4.5], [5.8], [8.0] and *Spitzer*/MIPS [24] bands.

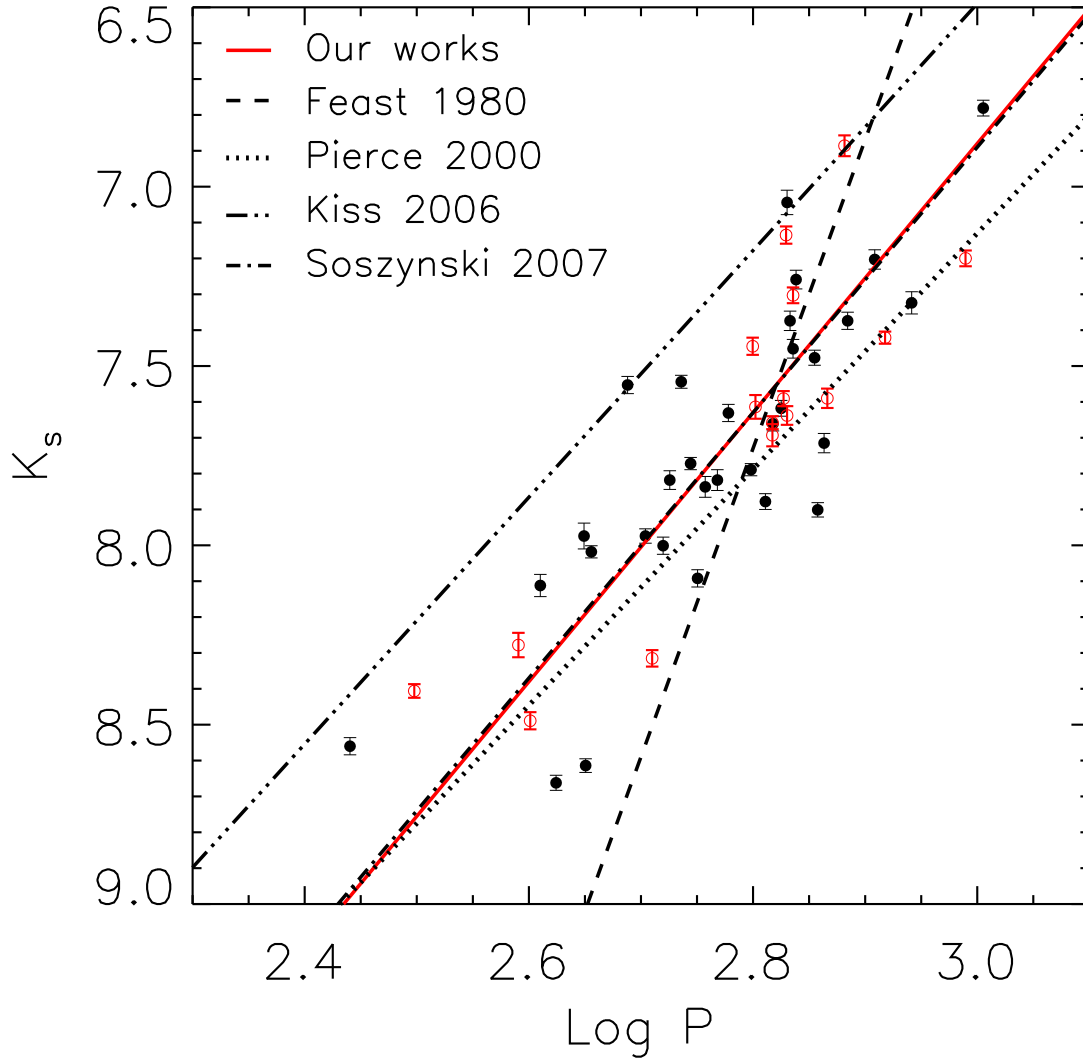


Fig. 13.— The P-L relation in the K_S band. The symbols have the same meaning as in Fig. 11, together with the measurement error bar in the K_S band. Also shown are the P-L relations for RSGs obtained by Feast et al. (1980), Pierce et al. (2000) and Kiss et al. (2006). The α_2 sequence for the AGB stars from Soszynski et al. (2007) is almost superposed on ours.

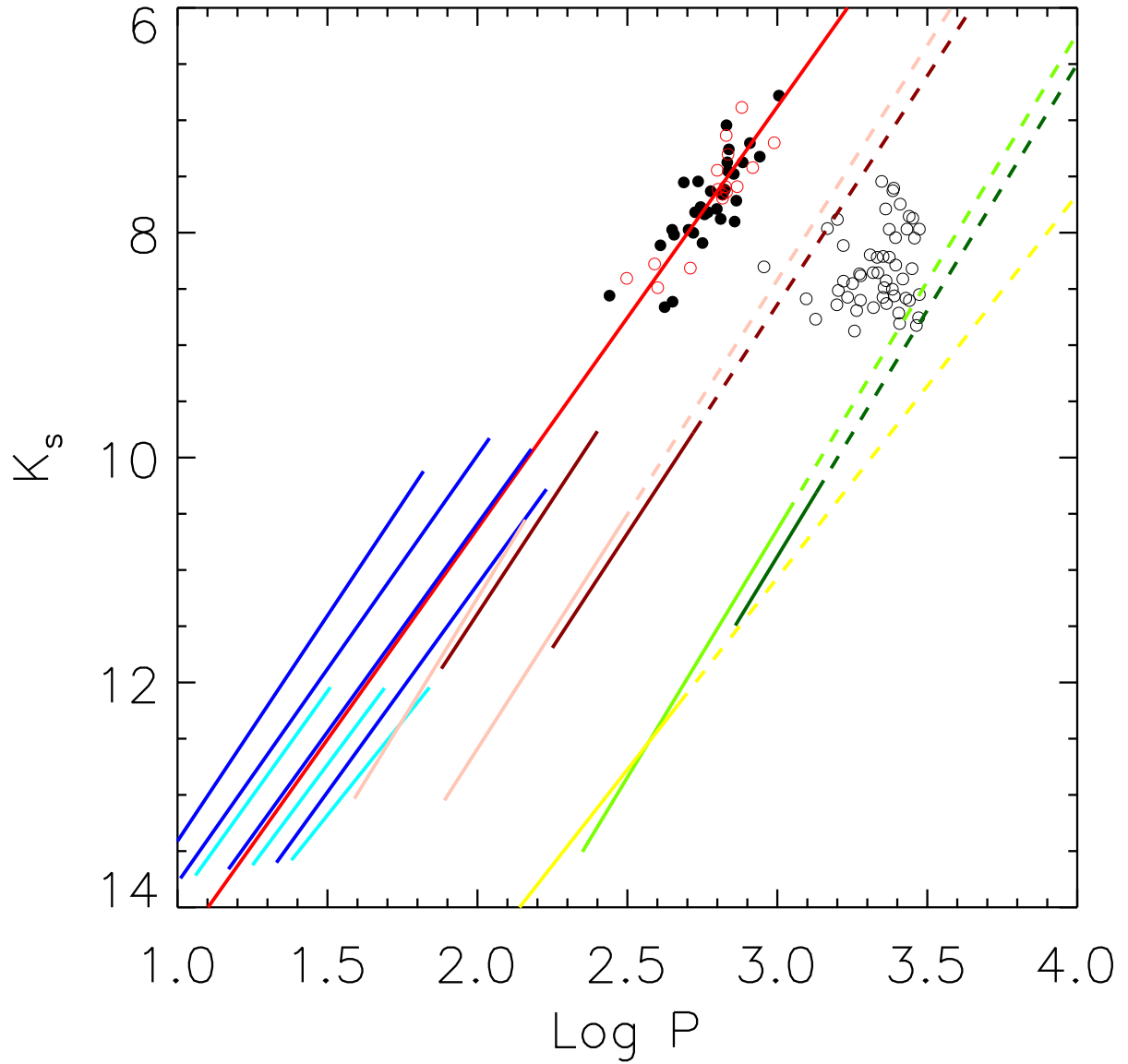


Fig. 14.— The K_S -band P-L relation for the semi-regular RSGs and LSP RSGs superposed on the P-L relations of LPVs in the LMC by Soszynski et al. (2007). The symbols obey the same convention as previous except that the newly added black open circle denotes the long secondary period of the LSP RSGs. The Soszynski et al. (2007) lines are the same as their Fig. 2.